

# A multimodal neural signature of face processing in autism within the fusiform gyrus

Received: 9 February 2024

Accepted: 7 October 2024

Published online: 2 January 2025

 Check for updates

A list of authors and their affiliations appears at the end of the paper

Atypical face processing is commonly reported in autism. Its neural correlates have been explored extensively across single neuroimaging modalities within key regions of the face processing network, such as the fusiform gyrus (FFG). Nonetheless, it is poorly understood how variation in brain anatomy and function jointly impacts face processing and social functioning. Here we leveraged a large multimodal sample to study the cross-modal signature of face processing within the FFG across four imaging modalities (structural magnetic resonance imaging (MRI), resting-state functional magnetic resonance imaging, task-functional magnetic resonance imaging and electroencephalography) in 204 autistic and nonautistic individuals aged 7–30 years (case–control design). We combined two methodological innovations—normative modeling and linked independent component analysis—to integrate individual-level deviations across modalities and assessed how multimodal components differentiated groups and informed social functioning in autism. Groups differed significantly in a multimodal component driven by bilateral resting-state functional MRI, bilateral structure, right task-functional MRI and left electroencephalography loadings in face-selective and retinotopic FFG. Multimodal components outperformed unimodal ones in differentiating groups. In autistic individuals, multimodal components were associated with cognitive and clinical features linked to social, but not nonsocial, functioning. These findings underscore the importance of elucidating multimodal neural associations of social functioning in autism, offering potential for the identification of mechanistic and prognostic biomarkers.

Autism is a lifelong neurodevelopmental condition with a prevalence of 1 in 36 children<sup>1</sup>. Social–communicative differences are among the most prominent features of autistic individuals<sup>2</sup>. In particular, difficulties with processing social information and faces, such as perceiving and interpreting facial expressions of emotions and other mental states, are thought to have a profound impact on their social functioning and daily living skills<sup>3,4</sup>. While nonautistic individuals (NAI) appear to develop highly skilled strategies to discriminate facial cues at a very early age, autistic individuals have been reported to

acquire less expertise with facial expression recognition<sup>5</sup>. This has, for example, been attributed to diminished social attention<sup>6</sup> and structural and functional differences in brain regions implicated in face processing<sup>3,5,7</sup>. While individual neuroimaging modalities have separately been used to characterize the neural correlates of face processing, multimodal studies of key regions associated with face processing remain scarce. Illuminating the rich multimodal information shared across different imaging modalities can unravel complex interactions and variations that may only be partially addressed by

✉ e-mail: [Dorothea.floris@uzh.ch](mailto:Dorothea.floris@uzh.ch)

single modalities<sup>8</sup>. Specifically, elucidating cross-modal links with regards to face processing in autism will be crucial for understanding the biological mechanisms associated with core social difficulties and paving the way for the development of more personalized support.

The fusiform gyrus (FFG) within the human ventral temporal cortex has been identified as a key neural region associated with higher-order processing of visual stimuli. The necessity for a thorough examination of the FFG in isolation is warranted by its detailed, functional heterogeneity exhibiting a fine-grained topographical organization with distinct category-selective patches<sup>9,10</sup> that are differentially specialized for facial recognition (that is, the fusiform face area (FFA))<sup>11</sup>, body part discrimination<sup>12</sup> and object features recognition<sup>13</sup>. With regards to face processing, the FFA in particular has increased activation during face perception tasks in functional magnetic resonance imaging (fMRI) studies<sup>14,15</sup> along with evidence from electroencephalography (EEG) studies showing an event-related potential of negative polarity that peaks at around 170 ms when facial stimuli are presented<sup>16,17</sup>. Furthermore, face processing is a lateralized cognitive function with right hemisphere dominance across these modalities<sup>18,19</sup>. An exhaustive examination across different neural signatures of this fine-grained local and hemispheric heterogeneity of the FFG—beyond the FFA—has yet to be conducted in autistic individuals. This can offer valuable new insights in light of reports of atypical functional specialization in autism<sup>20,21</sup>.

Accumulating evidence suggests that there is atypical neural organization within the FFG in autistic individuals. Many studies show that the FFG is hypoactive during face processing fMRI tasks<sup>22,23</sup> and functionally atypically connected<sup>24,25</sup> in autism. EEG studies show that the N170 latency is delayed in autistic individuals<sup>26,27</sup>. Structurally, there are reports of volume increases in right FFG<sup>28</sup>, a reduction in mean FFG neuron density<sup>29</sup> and reversed leftward asymmetry<sup>30</sup> in autism. These atypical neural substrates are thought to be functionally relevant in autistic individuals. For example, they have been linked to differences in facial expression recognition<sup>5</sup>, face memory<sup>31</sup>, adaptive social functioning<sup>27,32</sup> and social symptom difficulties and severity<sup>24,31,33,34</sup>.

While these individual imaging modalities (that is, structural MRI, task-fMRI, resting-state fMRI (rs-fMRI) and EEG) converge to show atypical involvement of the FFG in face processing and related social functioning in autism, there is still little research into how these different neural substrates jointly inform fine-grained FFG organization and social-communicative functioning in autism. Extracting common information from various modalities is crucial in gaining deeper insights into how brain structure and function reciprocally shape each other and inform behavior, cognition and clinical conditions, such as autism. So far, structure-function coupling has predominantly been addressed via univariate approaches where modalities are combined at the statistical or interpretation level<sup>27,35,36</sup>. However, only when employing multivariate multimodal approaches can we identify direct relationships between different neurobiological mechanisms and how they scale relative to each other. We can further penetrate across different biological spatial and temporal scales of variation leveraging the unique, complementary aspects covered by each individual imaging modality. Prior multimodal efforts are promising as they show that combining information from brain structure and function significantly increases accuracy in predictive frameworks<sup>37–41</sup>. Previous research in autism and other clinical populations, such as attention deficit hyperactivity disorder, bipolar disorder and schizophrenia shows that multimodal approaches can both replicate and extend unimodal results to shared pathophysiological processes<sup>42</sup> and even outperform unimodal approaches<sup>43–45</sup>. Additionally, a recent study combining different neuroimaging measures of rs-fMRI, diffusion-weighted imaging and structural morphometry specifically showed that resting-state (rs)-connection topographies within the FFG were differentially implicated between autistic and NAI<sup>46</sup>. While such multimodal endeavors are still scarce in autism, this work specifically underscores the important

role of the FFG in the neurobiology of autism. Still, the precise nature and a fine-grained topographical characterization of the multimodal neurobiological interactions within the FFG and their relationship with the broader clinical phenotype related to social functioning in autism remain to be established.

In the present study, our aim was to provide a more comprehensive understanding of the FFG in face processing in autism by elucidating the simultaneous involvement and multivariate interplay of different neural sources. Such analysis requires both large and deeply phenotyped samples, and given the scarce availability, especially in clinical populations, this has previously limited its application. Hence, in this study, we leveraged the unique, large-scale and deeply phenotyped EU-AIMS Longitudinal European Autism Project<sup>47,48</sup> (LEAP), which is the largest European multicenter initiative aimed at identifying biomarkers in autism. This dataset provides a rich set of different neuroimaging modalities and cognitive, clinical measures, as well as tasks related to face processing and social and nonsocial functioning. Differences in facial expression recognition in autistic individuals have been established in this dataset<sup>5</sup>. To further tap into their multimodal neural correlates, we combined two methodological innovations: (1) First, we employed normative modeling<sup>49</sup> on each imaging modality separately to derive individual-level deviations from a predicted age-related trajectory. Prior research shows that modeling cortical features as deviations from a normative neurodevelopmental trajectory provides a more sensitive measure to map multimodal signatures in psychopathology<sup>37</sup> while also improving predictive performance<sup>50</sup>. (2) Next, we conducted multimodal fusion through linked independent component analysis (LICA)<sup>51</sup> across structural MRI, rs-fMRI, task-fMRI and EEG within the right and left FFG to simultaneously decompose the imaging data into underlying modes that characterize multimodal signatures differentially in autistic and NAI. We further provided a fine-grained characterization of implicated regions, shedding light on the topographic organization within the FFG in autism. We hypothesized that multimodal components, by leveraging joint effects across different biological processes, would be more sensitive to capturing subtle diagnostic effects cross-modally. Consequently, they would outperform unimodal components in discriminating autistic from NAI. Finally, we hypothesized that joint expression across modalities related to the FFG and face processing would specifically inform social functioning in autism.

## Results

### Sample

For an overview of all methods see Fig. 1. The final sample of autistic ( $N = 99$ ) and NAI ( $N = 105$ ) did not differ significantly in sex ratio, age, measures of intellectual functioning, handedness, measures of structural image quality, number of EEG trials or head motion associated with task and rs-fMRI (Table 1).

### Unimodal normative models

First, unimodal normative models were estimated. Their accuracy was evaluated using the correlation between the true and the predicted voxel/time point values ( $\rho$ ), the explained variance (EV), the mean standardized log-loss and standardized mean squared error (Supplementary Fig. 1) and normative models per modality (Extended Data Fig. 1). Evaluation metrics were largely within recommended ranges<sup>52</sup> and highly similar when modeling age linearly (Supplementary Fig. 2). When testing for group differences in unimodal features, there were no significant differences in extreme  $Z$  deviations between autistic and NAI for any of the eight features (Supplementary Table 1).

### LICA

Next, the  $Z$  deviations (features) were merged using LICA<sup>51</sup>. In total, 50 independent components (ICs) were derived across eight different brain feature maps per hemisphere (that is, modalities)

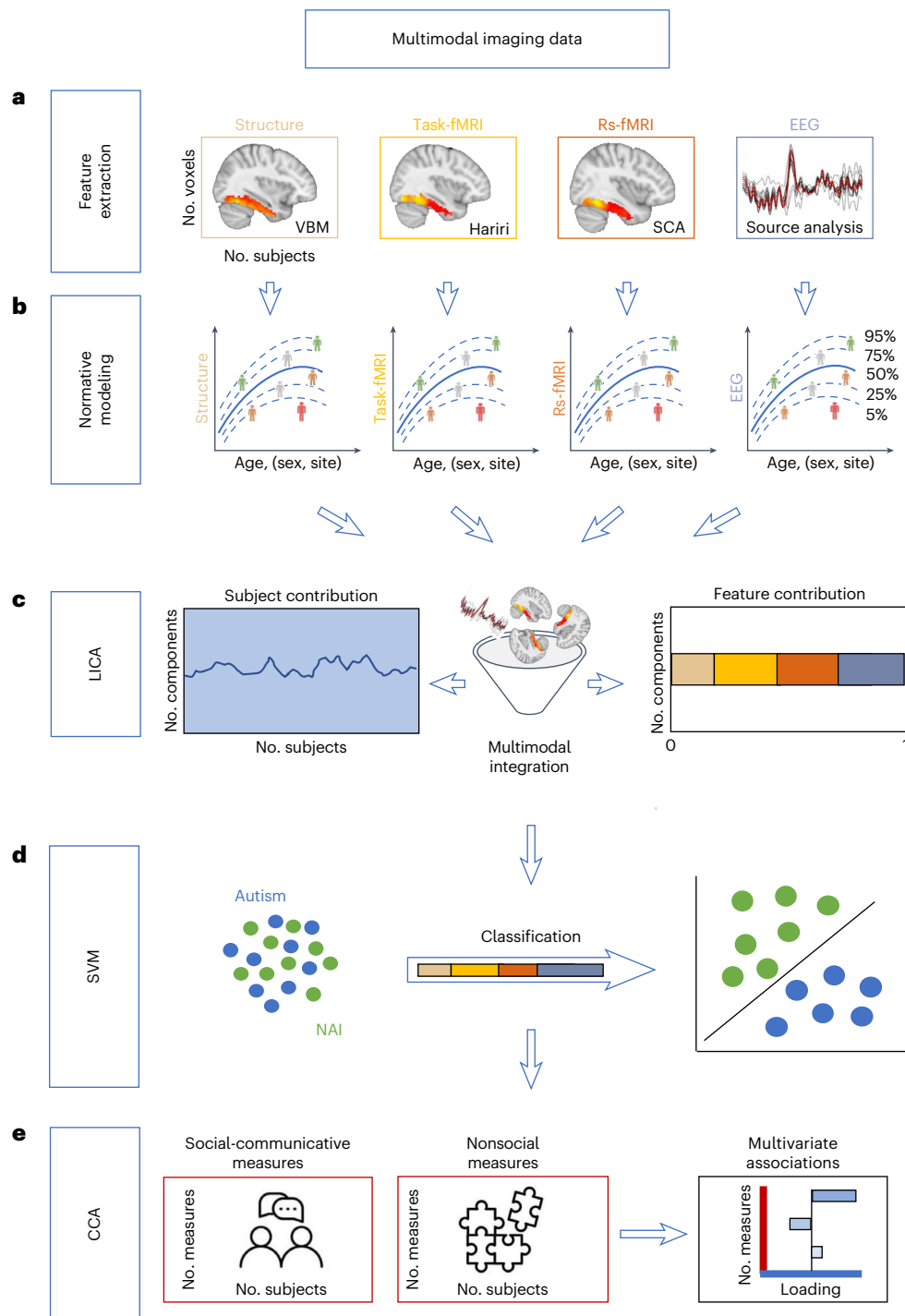


**Fig. 1 | Overview of the methodological approach.** **a**, The features for each modality were extracted from the right and the left FFG. These were (1) GM volume based on VBM for structural MRI, (2) T-maps contrasting the faces condition to the shapes condition reflecting sensitivity to faces from the Hariri paradigm for task-fMRI, (3) seed-based connectivity analysis (SCA) between the FFA and all other intra-FFG voxels for rs-fMRI and (4) the principal component of source-reconstructed time series for EEG. **b**, Next, normative modeling was applied to each imaging modality using Bayesian linear regression. The depicted trajectories per modality are schematic and the actual

modality-specific normative models are depicted in Extended Data Fig. 1. **c**, To model cross-subject individual-level variation, resulting Z-deviation maps per modality were statistically merged using LICA resulting in measures of modality contributions and subject loadings. **d**, Next, we tested for group differences in ICs and group separability using either multi- or unimodal ICs. **e**, Finally, we computed multivariate associations (that is, CCA) between subject loadings and clinical, cognitive measures related to either social-communicative or nonsocial features.

(Extended Data Fig. 2). Overall, across these, the right hemisphere (51.7%) and the left hemisphere (48.3%) did not contribute differentially. Single modality contributions were as follows: EEG R (35.0%) > EEG L (33.2%) > rs-fMRI R (11.2%) > rs-fMRI L (9.6%) > task-fMRI R (3.5%)

> task-fMRI L (3.4%) > structure L (2.1%) > structure R (2.1%). Supplementary Fig. 3 shows the correlations between the 50-dimensional factorizations (y axis) and 40 (Supplementary Fig. 3a) and 60 (Supplementary Fig. 3b) alternative dimensional factorizations. In line

**Table 1 | Demographic, clinical and imaging-related information of the sample**

| Variable              | Individuals with autism |       |           | NAI    |      |            | Post hoc              |
|-----------------------|-------------------------|-------|-----------|--------|------|------------|-----------------------|
| N                     | 99                      |       |           | 105    |      |            |                       |
| Sex                   | 71M                     | 28F   |           | 71M    | 34F  |            | $\chi^2=0.23, P=0.63$ |
|                       | Mean                    | S.d.  | Range     | Mean   | S.d. | Range      |                       |
| Age                   | 18.62                   | 5.32  | 7.58–30.0 | 18.3   | 4.87 | 10.37–30.9 | $t=0.44, P=0.66$      |
| FIQ                   | 107                     | 14.3  | 63–148    | 106    | 12.3 | 77–142     | $t=0.08, P=0.94$      |
| VIQ                   | 106                     | 15.62 | 51–160    | 107    | 14.1 | 74–142     | $t=0.09, P=0.93$      |
| PIQ                   | 107                     | 16.52 | 57–145    | 106    | 14.5 | 70–147     | $t=0.51, P=0.61$      |
| ADI social            | 14.54                   | 6.66  | 1.0–28.0  |        |      |            |                       |
| ADI communication     | 11.68                   | 5.66  | 0.0–26.0  |        |      |            |                       |
| ADI RRB               | 3.63                    | 2.41  | 0.0–12.0  |        |      |            |                       |
| ADOS CSS              | 5.06                    | 2.67  | 1.0–10.0  |        |      |            |                       |
| ADOS SA CSS           | 5.79                    | 2.7   | 1.0–10.0  |        |      |            |                       |
| ADOS RRB CSS          | 4.5                     | 2.49  | 1.0–10.0  |        |      |            |                       |
|                       | R                       | L     | A         | R      | L    | A          |                       |
| Handedness            | 88                      | 7     | 4         | 94     | 7    | 4          |                       |
|                       | Median                  | S.d.  | Range     | Median | S.d. | Range      |                       |
| QC structure          | 2.15                    | 0.11  | 2.04–3.0  | 2.13   | 0.19 | 1.96–3.42  | $W=4,926, P=0.52$     |
| Mean FD task-fMRI     | 0.09                    | 0.06  | 0.03–0.33 | 0.08   | 0.07 | 0.03–0.39  | $W=5,279, P=0.83$     |
| Mean D-VARS task-fMRI | 1.23                    | 0.14  | 0.9–1.74  | 1.24   | 0.16 | 0.83–1.61  | $W=5,392, P=0.56$     |
| Mean FD rs-fMRI       | 0.06                    | 0.05  | 0.03–0.27 | 0.06   | 0.06 | 0.02–0.4   | $W=4,915, P=0.5$      |
| Mean D-VARS rs-fMRI   | 1.96                    | 0.43  | 1.32–3.47 | 1.92   | 0.5  | 1.14–4.46  | $W=4,894, P=0.47$     |
| Number of EEG trials  | 90.6                    | 24.8  | 29–148    | 93.1   | 29.7 | 27–149     | $t=0.65, P=0.52$      |

Handedness was assessed with the short version of the Edinburgh Handedness Inventory. For sample characterization scores were categorized into right handed (+500 to +150), ambidextrous (−149 to +149) and left handed (−150 to −500). For structural QC measures, weighted overall image quality ratings ranging from 0.5 (best) to 10.5 (worst) were generated by the computational anatomy toolbox SPM pipeline. All variables did not significantly differ across autistic and NAI. Statistical comparisons were two sided. FIQ, full-scale IQ; VIQ, verbal IQ; PIQ, performance IQ; SA, social affect; CSS, calibrated severity scores; R, right handed; L, left handed; A, ambidextrous; QC, quality control; FD, framewise displacement in mm; D-VARS, root mean square of the temporal change of the fMRI voxel-wise signal at each time point (based on the raw images).

with previous reports<sup>53</sup>, most components were recovered with high accuracy independently of the order of the factorization.

### Group differences

Next, we compared the subject loadings of all (uni- and multimodal) ICs to test for differences between autistic and NAI. Among these, one multimodal IC (44) showed a significant group difference with autistic individuals having higher contributions than NAI ( $t = 3.5, P$  value of the false discovery rate (FDR) ( $P_{FDR} = 0.027$ ) (Fig. 2b). This remained unchanged when additionally controlling for handedness ( $t = 3.5, P_{FDR} = 0.028$ ) or when restricting analyses to right-handed individuals only ( $t = 3.7, P_{FDR} = 0.01$ ). There were no significant group differences in the remaining ICs (Supplementary Table 2) and no IC showed a significant association with handedness (Supplementary Table 3). The results further showed that there were no significant effects of site on group-differential IC44 (site 1:  $t = 0.37, P = 0.71$ ; site 2:  $t = 0.1, P = 0.92$ ; site 3:  $t = -0.78, P = 0.43$ ), nor were there any diagnosis by site effects (diagnosis  $\times$  site 1:  $t = 0.96, P = 0.34$ ; diagnosis  $\times$  site 2:  $t = 0.76, P = 0.45$ ; diagnosis  $\times$  site 3:  $t = 0.1, P = 0.92$ ). The significant multimodal component was not differentially driven by the right (52.8%) or left hemisphere (47.2%) and was associated with several functional modalities (rs-fMRI R (48.5%), rs-fMRI L (35.0%), EEG L (11.6%) and task-fMRI R (3.3%)), and to a smaller extent with gray matter (GM) volume (structure R (1.0%), structure L (0.5%)). Figure 3a depicts the spatial and temporal patterns for each imaging modality within IC44. When further characterizing these in terms of their anatomical and functional overlaps with the Harvard–Oxford atlas (HOA) (Fig. 3k) and the probabilistic functional atlas of human occipito-temporal visual cortex<sup>9</sup> (VIS) (Fig. 3f) in the

left hemisphere, autistic individuals showed more functional deviations than expected in rs-fMRI connectivity, primarily in retinotopic regions of occipital FFG while, to a smaller extent, also in lower-order face-selective regions (Fig. 3b,g). In the right hemisphere, they showed linked increased deviations in rs-fMRI and structure primarily in higher-order face (mid-lateral fusiform gyrus, mFus, also referred to as FFA-2; posterior lateral fusiform gyrus, pFus, also referred to as FFA-1) and bodies-selective regions of temporal-occipital and occipital FFG (Fig. 3c,h). On the other hand, regions in the left hemisphere where autistic individuals showed linked decreased deviations across structure and rs-fMRI compared with NAI localized to both higher-order face-selective (mFus, pFus) and retinotopic regions of posterior, temporal-occipital and occipital FFG (Fig. 3d,i). In the right hemisphere, these were mostly in higher-order face-selective regions (pFus) across rs-fMRI and task-fMRI and in retinotopic regions across structure in occipital FFG (Fig. 3e,j). Furthermore, autistic individuals showed more left EEG source activation than expected, around 195–203 ms and 417–426 ms, whereas less source activation at 444–449 ms than expected. For further details see Supplementary Table 4.

### Multimodal components

For further analyses, we focused on multimodal components only by excluding those that were primarily driven by one imaging modality (that is, with a multimodal index (MMI) below 0.1; Methods and Supplementary Fig. 4) resulting in 11 multimodal ICs (Fig. 2a). Across these multimodal ICs, the right hemisphere (60.0%) contributed more than the left hemisphere (40.0%). Single modality contributions across all multimodal ICs were as follows: EEG R (26.3%) > rs-fMRI R (19.7%) >



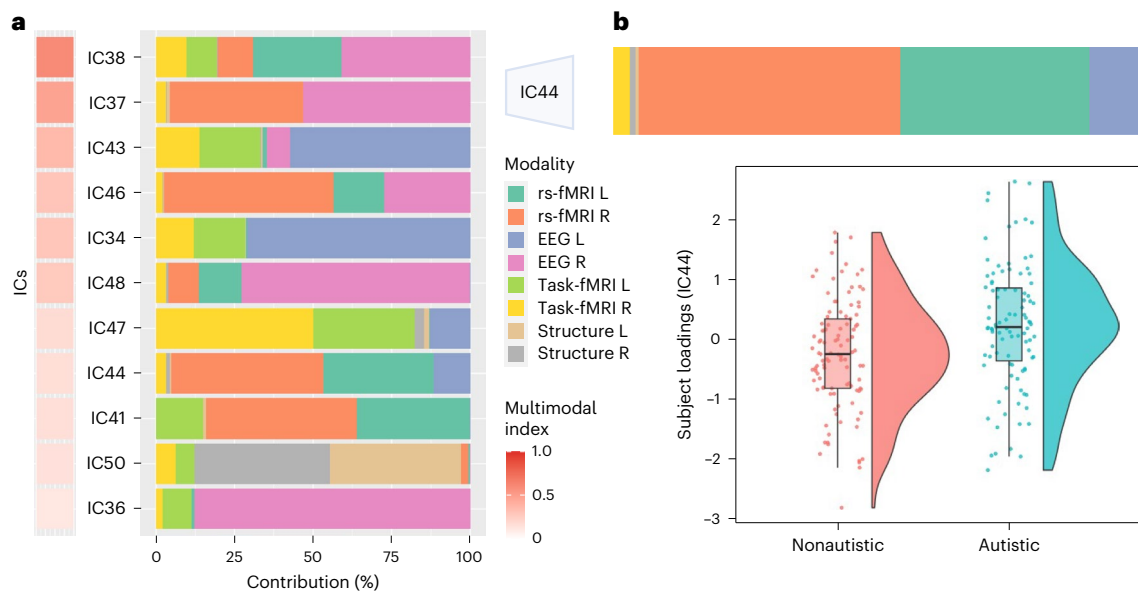


**Fig. 2 | Multimodal components and group differences in IC44. a**, Among all ICs, 11 were considered multimodal (Fig. 2a), with a single modality contribution of not more than 90%. **b**, The violin plots display the distribution of subject loadings (IC44) for autistic and NAI. IC44 showed a significant group difference

with autistic individuals ( $N = 99$ ) having higher contributions than NAI ( $N = 105$ ). The box plot shows the median and the interquartile range (that is, the 25th and 75th percentiles) with whiskers extending to 1.5 times the interquartile range from the first and third quartiles. L, left; R, right.

EEGL (13.9%) > rs-fMRIL (12.1%) > task-fMRIL (9.8%) > task-fMRIR (9.6%) > structure R (4.4%) > structure L (4.2%).

### Autism classification

Next, we applied a support vector machine (SVM) to compare the efficacy of unimodal and multimodal ICs in differentiating between the two diagnostic groups. The results showed that multimodal ICs performed significantly better at discriminating autistic from NAI (area under the receiver operating characteristic curve (AUC) unimodal of 0.48, AUC multimodal of 0.64,  $P < 0.001$ ). This result was confirmed across a range of different multimodality thresholds (Extended Data Fig. 3a) and was not influenced by varying numbers of features between multimodal and unimodal ICs (Extended Data Fig. 3b).

### Clinical and cognitive associations

To test for brain–behavior relations, we ran canonical correlation analysis (CCA). This revealed a significant multivariate association between the multimodal ICs and social–communicative features (that is, autism diagnostic observation schedule (ADOS) social affect<sup>54</sup>, autism diagnostic interview (ADI)-social<sup>55</sup>, ADI communication, Vineland adaptive behavior scale<sup>56</sup> with communication, daily living, socialization subscales, the Reading the Mind in the Eyes Test (RMET)<sup>57</sup> and Hariri faces task<sup>58–60</sup>) ( $r = 0.65$ ,  $P_{FDR} = 0.008$ ; Fig. 4b). This remained unchanged when additionally controlling for handedness ( $r = 0.65$ ,  $P_{FDR} = 0.002$ ) or when restricting analyses to right-handed individuals only ( $r = 0.66$ ,  $P_{FDR} = 0.002$ ). On the other hand, the relationship between the multimodal ICs and nonsocial features (that is, ADOS restrictive and repetitive behavior (RRB), ADI RRB, the Repetitive Behavior Scale (RBS)<sup>61</sup>, the systemizing quotient (SQ)<sup>62–64</sup> and Hariri shape-matching condition) was not significant ( $r = 0.45$ ,  $P_{FDR} = 0.64$ ; Extended Data Fig. 4) pointing to specificity with social-related features of multimodal ICs. These associations remained stable when varying the multimodality threshold (Supplementary Fig. 5). For the significant associations, multimodal IC37 showed the largest contribution on the imaging side followed by IC38, IC44 and IC34 (Fig. 4a,c), whereas ADOS social affect, RMET and Hariri face matching scores showed the largest contribution on the behavioral side (Fig. 4d). The ICs contributing most are depicted in Fig. 4c and Supplementary Figs. 6–8. On average, the right (56.5%) and

the left hemisphere (43.5%) did not contribute differentially to these four ICs, which were mostly driven by all functional modalities. Next, imaging patterns correlating with social communication features were characterized in terms of their overlap with anatomical and functional overlaps with the HOA and VIS atlases (Fig. 4e and Supplementary Fig. 9). Especially in higher-order face-selective regions (mFus and pFus) of posterior and temporal-occipital FFG, there were both linked increased deviations in bilateral rs-fMRI and task-fMRI and linked decreased deviations in bilateral structure and right rs-fMRI connectivity. At the same time, particularly in retinotopic regions of occipital FFG, there was more bilateral GM volume along with less right task activation than expected. There were more deviations in right EEG source activation at around 290 ms, while left EEG did not reach significance. These joint imaging patterns were associated with more social difficulties as assessed by the ADOS, ADI and Vineland, and more errors on the RMET, while also with greater accuracy on the Hariri faces task. For more details, see Supplementary Tables 5–8.

## Discussion

In the present study, we aimed to characterize the multimodal neural signature of face processing in autism within the FFG, the core region of the face processing network. We identified several ICs that were differentially associated with the four modalities (structure, rs-fMRI, task-fMRI and EEG), hemispheres and functional subdivisions of the FFG. Autism-associated differences in FFG organization were more pronounced when penetrating across multiple rather than single modalities. Furthermore, a set of multimodal ICs was associated with core features related to social but not nonsocial functioning in autism. Taken together, these findings highlight the value of cross-modal analyses in characterizing a key structure in the multilevel neurobiology of autism and its implication in core cognitive and clinical features.

### Group differences

Among all components, one multimodal component (that is, IC44) showed a significant difference in subject loadings between autistic and NAI. Overall, the right and left hemispheres did not show differential contributions within this IC and it was associated with all modalities fed into the analysis, with the functional modalities, especially rs-fMRI

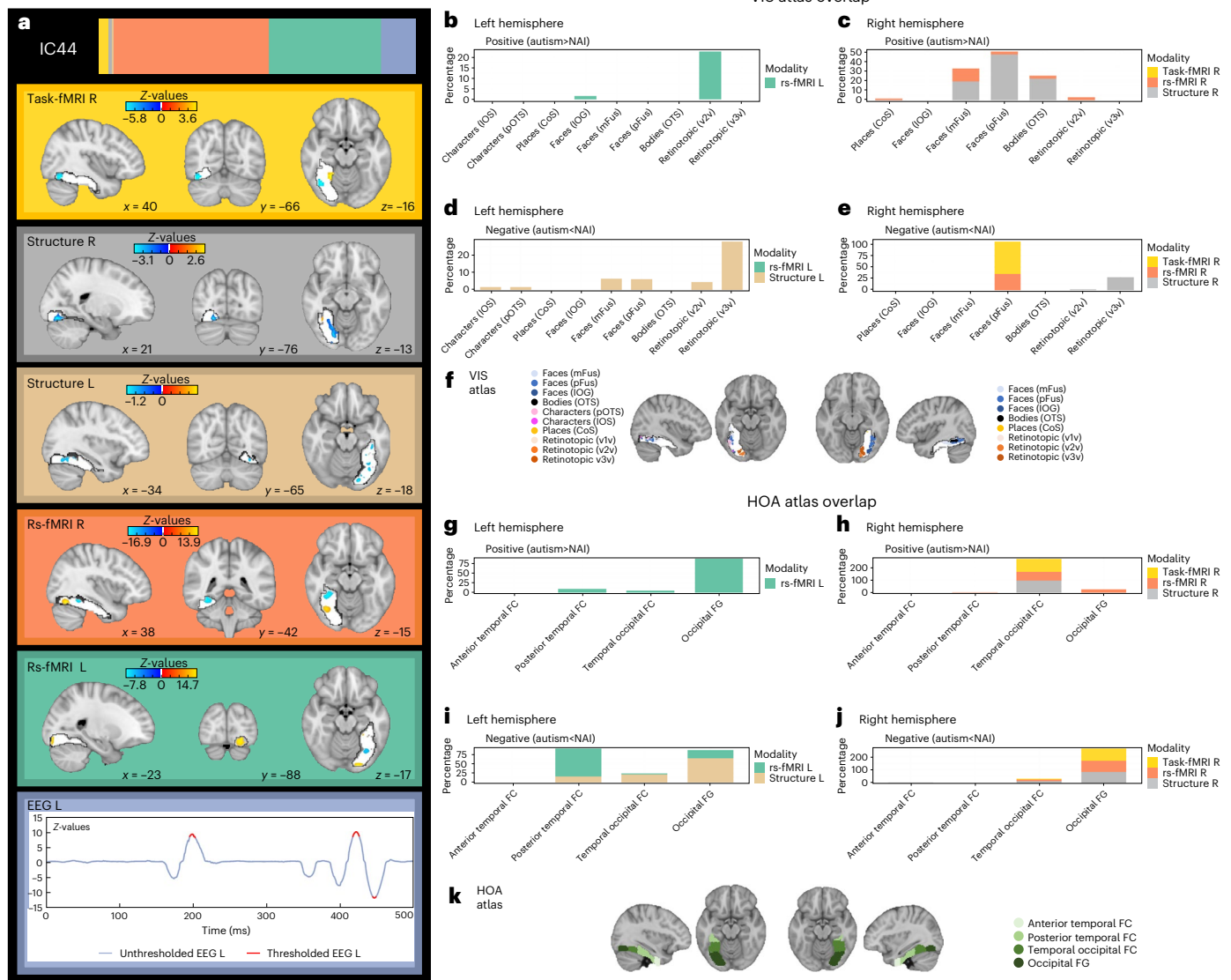


**Fig. 3 | Spatial and temporal characterization of IC44.** **a**, The spatial and temporal Z-maps thresholded at the 95th percentile of the different modalities associated with IC44. Positive values (yellow) depict positive loadings onto the IC where autistic individuals have higher deviations than NAI. The negative values (blue) depict negative loadings onto the IC where autistic individuals have lower deviations than NAI. Suprathreshold time points for EEG are depicted in red. **b–e**, The spatial overlap of suprathreshold voxels with a probabilistic functional atlas of the occipito-temporal cortex (that is, VIS atlas<sup>9</sup>) for the positive loadings (that is, autism > NAI) (**b** and **c**) and negative loadings (that is, autism < NAI) (**d** and **e**), for the left (**b** and **d**) and right (**c** and **e**) hemispheres. **f**, The VIS atlas

and its different category-selective subregions. **g–j**, The spatial overlap of suprathreshold voxels with the structural HOA (depicted in **k**) for the positive loadings (**g** and **h**) and the negative loadings (**i** and **j**), for the left (**g** and **i**) and the right (**h** and **j**) hemispheres. **k**, The HOA and its four FFG subregions (that is, anterior and posterior divisions of the temporal FC, temporal-occipital FC and occipital FG. CoS, collateral sulcus; FC, fusiform cortex; IOG, inferior occipital gyrus; IOS, inferior occipital sulcus; OTS, occipital temporal sulcus; pOTS, posterior OTS; VIS, probabilistic functional atlas of the occipito-temporal cortex; R, right; L, left. v1v, v2v, v3v are ventral topographic regions in early visual cortex.

and EEG, contributing most (Fig. 3). In particular, the overlap with the VIS atlas highlighted that face-selective and retinotopic regions of the FFG were most different between autistic and NAI. More specifically, in the right hemisphere, higher-order face-selective regions exhibited less task activation and FFA connectivity in autistic individuals than expected, primarily in occipital FFG areas (Fig. 3e,j). At the same time autistic individuals showed increased deviations in FFA connectivity primarily in temporal-occipital FFG along with increased GM volume deviations in higher-order face-selective FFG regions (Fig. 3c,h). This strong right-hemisphere involvement of regions associated with FFA across several modalities is in line with reports of increased FFA volume<sup>28</sup> and decreased FFA task activation<sup>65,66</sup> and FFA connectivity<sup>24,67</sup> in autism. Similarly, temporally, autistic individuals showed more

increased left deviations around 195 ms, potentially indicative of the consistently reported finding of a slower N170 in autistic individuals<sup>26</sup>. This has specifically also been shown and extensively characterized in the current sample<sup>27</sup>. Together these patterns converge to point toward autism-associated differences in face-selective areas of the FFG, at the structural, functional and temporal levels. While these results align with earlier unimodal discoveries, it was previously uncertain whether disparate signals would be separate and independent from each other or coalesce into a joint multimodal expression. Only by employing multimodal approaches are we able to identify the direct links between different neurobiological mechanisms and comprehend how they scale relative to one another while also leveraging the complementary aspects conveyed by each individual imaging modality. In this context,

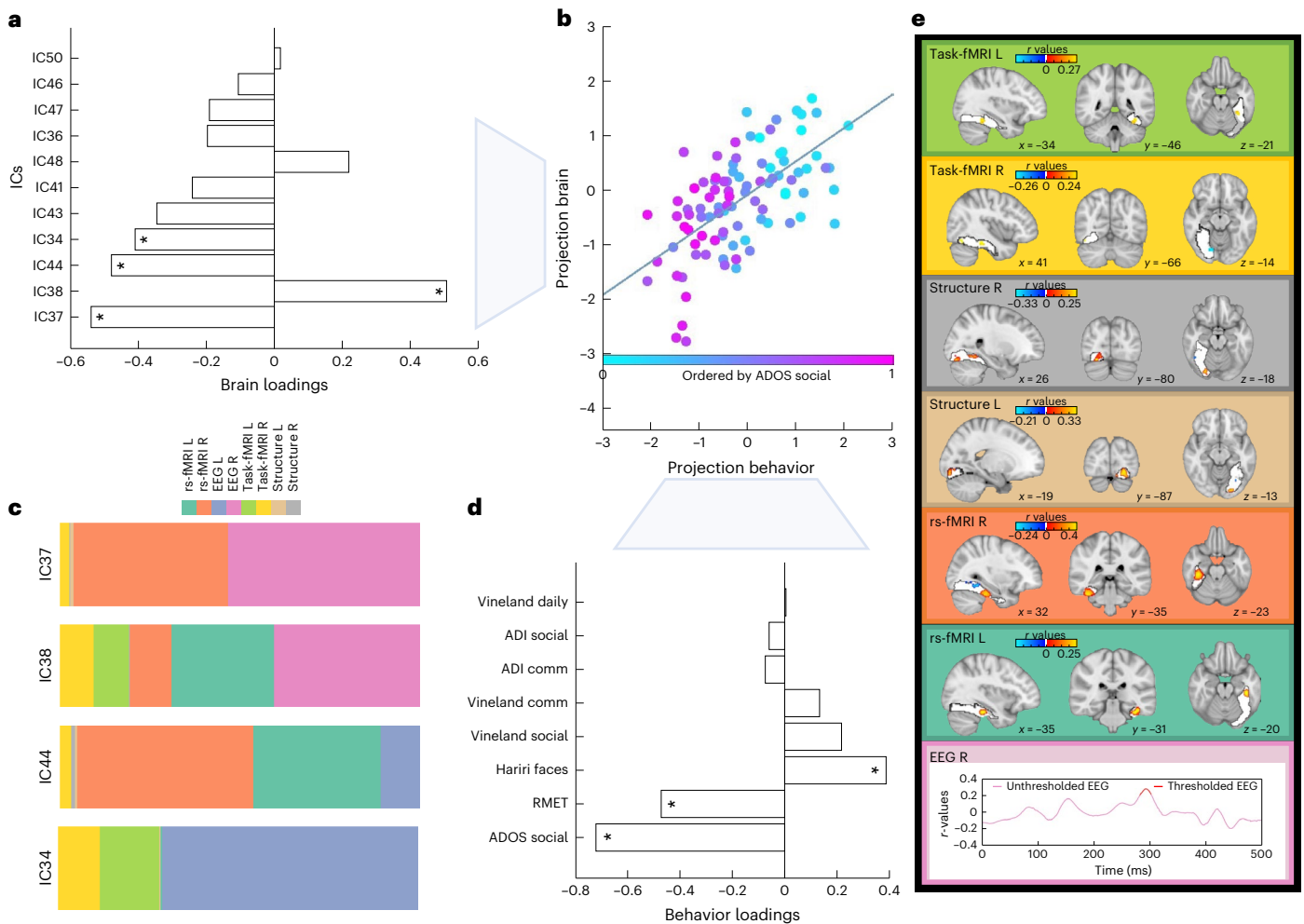


**Fig. 4 | CCA between the multimodal ICs and social-communicative features.** The multivariate association (that is, canonical correlation) was significant between the 11 multimodal ICs and the social-communicative features associated with autism. **a**, The loadings of each multimodal component contributing to the CCA mode. **b**, The canonical correlation scatter plot color coded by the highest contributing clinical feature (ADOS social affect). The x axis depicts the projected behavioral CCA variate (projection behavior) and the y axis the multimodal ICs CCA variates (projection brain). **c**, The modality contributions of the four ICs that contribute significantly to the CCA. **d**, The

loadings of each social-communicative feature contributing to the CCA mode. The asterisks show the significant loadings. **e**, The spatial and temporal patterns of each imaging modality that are significantly correlated with the social-communicative features. These are based on the significant correlation values between the Z deviations of each imaging modality and the canonical imaging variate derived from the CCA. ADOS social, ADOS social affect subscale; ADI comm, ADI communication subscale; Vineland daily, Vineland daily living skills subscale; Vineland comm, Vineland communication subscale; Vineland soc, Vineland Socialization subscale; R, right; L, left.

we provide evidence supporting the interconnected nature of distinct signals within a single unified framework.

In the left hemisphere, IC44-related increased deviations in EEG source activation at around 420 ms may indicate reductions in the face N400, which has been associated with familiar face recognition and semantic information<sup>68</sup>. While in NAI, face processing becomes the most highly developed visual skill, autistic individuals may find social stimuli less rewarding (that is, less socially motivating), resulting in faces potentially conveying greater novelty and thus decreased familiarity<sup>69</sup>. Furthermore, occipital, retinotopic areas of the left FFG were most implicated as shown by increased functional connectivity deviations between the FFA and retinotopic and lower-order face-selective areas of the FFG in autistic individuals (Fig. 3b,g). This was echoed by less GM volume than expected in left retinotopic areas of FFG in autistic individuals (Fig. 3d,i). Retinotopic early visual areas act as the first stage in a hierarchical network of face processing in which lower-level feature-based components are processed before more complex features in higher-order face-selective regions<sup>70</sup>. Neural deviations in early visual areas, as seen here, are in line with reports

of autistic individuals showing differences in sensory processing at early perceptual stages and have been described at the cognitive level as weak central coherence<sup>71</sup>. Accordingly, studies show that autistic individuals exhibit a different strategy in processing facial and visual stimuli with a stronger focus on featural, local aspects at the expense of holistic, global information<sup>72</sup>. Similarly, fMRI studies converge to show greater feature-based perceptual strategies in autistic individuals who primarily tend to recruit object-related regions<sup>73,74</sup> when viewing facial stimuli. Taken together, this suggests that the differences we discovered in the left hemisphere point primarily to low-level, bottom-up processing differences, whereas in the right hemisphere they may indicate higher-level atypicalities in the FFA, with a differential involvement across the different structural and functional modalities.

**Clinical and cognitive associations**

Multimodal ICs showed a significant association with a set of clinical and cognitive features associated with social functioning in autism (Fig. 4). Group-differential IC44 was also among the ICs contributing significantly to these associations. Components loading significantly



onto the CCA were mostly driven by functional modalities. Right EEG source activation deviations were around 280–300 ms, potentially indicative of the N250r generated in the FFG<sup>75</sup> and associated with the repetition of familiar facial stimuli<sup>76</sup>. The amplitude of the N250r has been shown to decrease with increasing working memory load<sup>77</sup>. This suggests that the increased deviations seen here in autistic individuals may reflect differences in degrees of working memory resources allocated to the processing of facial stimuli, which appear more novel and require more attentional effort in autistic individuals. This increased cognitive demand may indicate that the reduced reward response to social stimuli in autism leads to less automatic and more effortful processing of faces<sup>69</sup>. With regards to the other modalities, increased deviations particularly in higher-order face-selective regions across brain function (task-fMRI and rs-fMRI) while also in lower-order early visual regions across brain structure were associated with more autistic features, such as more social difficulties as assessed by ADOS and lower social sensitivity as assessed by the RMET. Previous unimodal studies showed that the delayed latency of the N170 predicts change in social adaptive behavior in autistic individuals<sup>27</sup> (that is, EEG), autistic individuals with low performance on facial emotion recognition have reduced bilateral FFG activation (that is, task-fMRI)<sup>5</sup> and that atypical FFA connectivity is associated with increased social symptom severity in autism (that is, rs-fMRI)<sup>24</sup>. Here, we extend the unimodal results to a multivariate association across a range of social–communicative features that are related to cross-modal signatures within the FFG. Previously, it was unclear whether these separate neural signals contribute independently or jointly to social–communicative features in autism. Our findings provide evidence for an interrelated biological basis of core social functioning in autism and demonstrate that appropriately modeling shared variance across different modalities increases sensitivity to clinical–cognitive features associated with autism<sup>78</sup>. Remarkably, at the same time, there was no association with a set of nonsocial features, such as repetitive behaviors, pointing to specificity of these multimodal ICs with regards to social functioning.

### Summary and implications

Taken together, the multimodal neural signature within the FFG in autism presents differentially across hemispheres, modalities and topography. Specifically, the picture emerges that (1) the functional modalities contribute more than the structural modalities and (2) retinotopic, occipital regions are more implicated in the left hemisphere and higher-order regions are more implicated in the right hemisphere within the FFG when it comes to group differences, but they do not contribute differentially with regards to social functioning. (1) Concurrent neural activity and functional co-expressions (task-fMRI, rs-fMRI and EEG) were strongly tied to social features observed in autistic individuals at present (such as current performance and ADOS assessment). On the other hand, more stable structural aspects of the brain established over time, as well as historical symptoms reported through the ADI and Vineland—which provide insights into past behaviors—had a comparatively smaller impact on the observed association. These results highlight the dynamic nature of the relationship between neural activity and social functioning in autism, underscoring the importance of considering the temporal dimension when investigating the neural correlates of social functioning in autism. Future putative neuroscientifically informed interventions targeting social features may thus benefit from a focus on concurrent neural functioning. (2) Topographically, the FFG is known to exhibit an anterior to posterior gradient with more posterior regions related to lower-order, early visual processing, and more anterior regions related to higher-order processing<sup>79</sup>. Here, we see the involvement of both retinotopic and higher-order cognitive, particularly face-sensitive, patches. This points to differences in both bottom-up perceptual processes and top-down cognitive information processing in face processing in autism, which can amount to a difference in the face processing strategy employed (for example, more

feature based), and which has extensively been described in autism as weak central coherence<sup>71</sup>. These different processing levels are not differentially implicated across hemispheres in the processing of social information in autism, suggesting that the distinctive face processing strategy in autism transcends right hemisphere dominance of face processing. On the other hand, hemispheric differences are more apparent in the group-differential IC. Teasing apart hemispheric contributions is particularly important in the light of reports of atypical patterns of brain asymmetry in autistic individuals<sup>21,34,80</sup>. More extreme deviations from a normative model have, for example, been reported in right temporal-occipital fusiform cortex asymmetry in autistic females<sup>21</sup>, along with more left-lateralized volume in posterior temporal FFG in autistic individuals<sup>30,34</sup>. Subsequent research should further explore these more nuanced insights revealed by cross-modal analyses pointing to left-lateralized low-level and right-lateralized high-level differences between autistic and NAI.

### Strengths and limitations

Integrating data from different modalities has the advantage of being biologically more informative and comprehensive in characterizing a complex, heterogeneous condition, such as autism. Accordingly, when comparing unimodal deviations in each imaging modality, as well as comparing predominantly unimodal ICs between autistic and NAI, there were no significant group differences, despite employing more sensitive individual-level measures derived from normative modeling. Additionally, in line with previous studies<sup>43–45</sup>, multimodal features significantly outperformed unimodal features in differentiating autistic from NAI. As shown, this difference in predictive performance between unimodal and multimodal features is not solely dependent on the quantity of information provided by each modality, but rather on the relevance and complementary nature of the features from different modalities. This suggests that the improvement in classification depends on the specific characteristics and interplay of the features involved. Together, these results confirm our hypothesis and align with previous reports<sup>78,81</sup> that appropriately modeling cross-modal variance increases sensitivity to detecting subtle effects that may otherwise be missed. It is important to note, however, that the inclusion of multimodal features does not automatically guarantee superior performance. In certain scenarios, one single modality may suffice, especially when it captures a pronounced biological effect, and adding other modalities could introduce noise rather than biological information. Thus, the superiority of multimodal over unimodal approaches depends on the presence of biologically meaningful, shared information across the modalities. This is particularly relevant for complex cognitive functions, such as face processing, where multiple cellular processes and biophysical changes that manifest across various modalities are involved. These findings further suggest that the discerning signals in this specific brain region are reliably captured through components shared across modalities, emphasizing the multidimensional nature of social functioning associated with autism. Thus, integrating different structural and functional brain measures is among the most promising and powerful methods to achieve substantial advances in our understanding of system-level atypicalities in autism and provides the basis for elucidating mechanisms through which interventions can most efficiently improve clinically relevant functioning<sup>78</sup>. Furthermore, we combine different innovative methods: LICA is particularly powerful when modeling modalities that are different in their numbers of features, spatial correlations, intensity distributions and units. This is because LICA optimally weighs the contributions of each modality by correcting for the number of effective degrees of freedom and the use of automatic relevance determination priors on components<sup>8,51,78</sup>. Moreover, by combining normative modeling with LICA, we employ a previously validated approach that has been shown to increase sensitivity in detecting cross-modal effects in clinical populations<sup>37</sup>.



At the same time, it needs to be pointed out that face processing involves an extended neural network across the whole brain, including other structures such as the amygdala, superior temporal sulcus and occipital and frontal cortex<sup>37,74,82,83</sup>. It may thus seem too simplistic to reduce face processing to a single brain region. However, the FFG is claimed to be the core node of a distributed face processing network, as substantiated by FFG lesion studies<sup>84,85</sup>, and its fine-grained functional heterogeneity warrants careful examination in isolation. Additionally, implementing cross-modal analyses presents additional challenges, such as obtaining sufficiently large sample sizes with all participants having available data across all imaging modalities. Here, from a sample of over 600 individuals in the EU-AIMS LEAP dataset, we were able to conduct an analysis in just over 200 individuals who had available imaging data across the four different modalities. Whole-brain analyses based on multivariate techniques will ultimately require larger sample sizes. In the same context, although our prior work suggests that face processing is related to sex-differential factors in autism<sup>86</sup>, in the current study we did not run sex-stratified analyses owing to the small number of female participants. Future studies with larger sample sizes of both sexes should investigate this further. Furthermore, previous studies have linked handedness with face processing, particularly showing an association between atypical lateralization and left handedness<sup>87,88</sup>. Owing to the small number of left-handed or ambidextrous individuals in our sample, it is not surprising that we did not find an association with handedness. Still, future research should explore this question in the context of autism. Moreover, there is variability across studies in the task paradigms and comparison stimuli they employ for localizing face processing-related activation. Comparison stimuli vary in the degree to which they resemble living objects or faces (for example, geometrical shapes, houses, scenes, scrambled stimuli and grebles) or in their state (dynamic versus static stimuli). Differences in these stimuli have been shown to produce variability in the extent, strength and patterns of the activation in the FFG<sup>89,90</sup>. While the localization and peak location of the FFA are relatively unaffected by the specific task and comparison stimuli employed<sup>89</sup>, it is important to acknowledge that the choice of comparison stimuli is a limitation, which may affect the face specificity of task-based findings. For example, comparison stimuli with face-like features may increase specificity toward face processing. Thus, while future studies should investigate which paradigms and comparison stimuli are most sensitive to elicit autism-related differences in face processing-related FFA activation, we are confident that the functional responses within the FFG observed in our study can be largely attributed to the processing of face-like features. Finally, while both unimodal and more easily implemented behavioral tools, such as eye-tracking, continue to play an important role in the diagnostic process and biological characterization of autism<sup>91,92</sup>, integrating and supplementing these with multimodal approaches can enhance diagnostic accuracy and offer deeper insights into the multifaceted, biological underpinnings of the condition.

## Conclusions

Integrating information from multiple imaging modalities allows us to gain a more holistic and robust understanding of the complex neural processes underlying core clinical and cognitive features associated with autism. The present results suggest that the FFG is a central region differentially implicated across different neural signals and category-selective regions in autistic and NAI and that this cross-modally informs the mechanisms associated with core social functioning in autism. Eventually, elucidating more precise, integrated and individual-level neural associations of core cognitive and clinical features will pave the way for further work identifying stratification, mechanistic and prognostic biomarkers and the development of more personalized support, thereby eventually improving the quality of lives of autistic individuals.

## Methods

### Sample characterization

Participants were part of the EU-AIMS/AIMS-2-TRIALS LEAP cohort<sup>47,48</sup>. They underwent comprehensive clinical, cognitive and MRI assessment at one of six collaborating sites. All autistic participants had an existing clinical diagnosis of autism that was confirmed using the combined information of gold-standard diagnostic instruments, the ADI revised<sup>55</sup> and the ADOS<sup>93,94</sup>. The study was approved by the respective research ethics committees at each site (via the Integrated Research Application System; Supplementary Table 9). Informed written consent was obtained from all participants or, for minors or those unable to give informed consent, from a parent or legal guardian. Participants did not receive compensation for study visits. Exclusion criteria included the presence of any MRI contraindications (for example, metal implants, braces or claustrophobia) or failure to give informed written consent to MRI scanning, as well as substantial hearing or visual impairments not corrected by glasses or hearing aids. Individuals with an intelligence quotient (IQ) below 50 were excluded. In the autistic group, psychiatric conditions (except for psychosis or bipolar disorder) were allowed, while in the NAI group, parent or self-report of a psychiatric disorder was an exclusion criterion. A history of alcohol and/or substance abuse or dependence in the past year was an exclusion criterion for both groups. Individuals were included if they were on stable medication (at least 8 weeks) at entrance point and over the course of the baseline visit. For further details on the sample and exclusion and inclusion criteria, see Supplementary Methods and our earlier papers<sup>47,48</sup>. For inclusion and exclusion criteria per modality, see Supplementary Methods and Extended Data Fig. 5. The final sample has both complete imaging data across four different imaging modalities and phenotypic information available consisting of 99 autistic (71 males, 28 females) and 105 NAI (71 males, 34 females) between 7 and 30 years (Table 1). For a distribution of FIQ and handedness, see Supplementary Figs. 10 and 11, for information on the ethnicity of participants, see Supplementary Table 10, and on medication use, see Supplementary Table 11.

### Clinical and cognitive measures

We split available autism-associated measures into two sets of feature sets on the basis of the construct they measure (1) social-communicative features comprising measures of difficulties with social communication and daily living skills (that is, ADOS social affect, ADI communication, ADI social, Vineland adaptive behavior scale<sup>56</sup> with communication, daily living and socialization subscales), face matching performance (that is, Hariri faces task<sup>58-60</sup>) and social sensitivity to complex emotions (that is, RME<sup>57</sup>) and (2) nonsocial features comprising RRBs (that is, ADOS RRB and ADI RRB, the RBS<sup>61</sup>), systemizing (that is, the SQ<sup>62-64</sup>) and shape-matching performance (that is, Hariri shapes task, as the control condition to the Hariri faces task) (Supplementary Methods and Supplementary Table 12). To tackle missing clinical data and to further avoid reducing the sample size, we used imputed clinical data (derived from Extra Trees regression)<sup>95</sup>, as in previous work with this dataset<sup>41,96</sup>.

### ROI for FFG

All analyses were restricted to the right and left FFG on the basis of the HOA (Oxford Center for Functional MRI of the Brain) adjusted to have 100% coverage across all individuals for each imaging modality (Supplementary Methods).

### Imaging modalities

For MRI and EEG data acquisition parameters and detailed preprocessing steps per modality, see Supplementary Methods and Supplementary Tables 13–14. In summary, the features for subsequent normative modeling were as follows (1) structure: voxel-based morphometry (VBM)-derived, voxel-wise GM volumes, (2) rs-fMRI: seed-based correlation between the FFA and the remaining FFG, (3) task-fMRI: T-contrast

maps reflecting sensitivity to faces and (4) EEG: the principal component of source-reconstructed activation obtained across different cortical FFG parcels.

### Normative modeling

Normative modeling is an emerging statistical technique that allows parsing heterogeneity by charting variation in brain–behavior mappings relative to a normative range and provides statistical inference at the level of the individual<sup>97</sup>. The term ‘normative’ should not be seen as incompatible with the neurodiversity framework as it simply refers to statistical norms, such as growth charts, that vary by demographics, such as age and sex. Here, we trained normative models using Bayesian linear regression<sup>98</sup> for each brain imaging modality within the right and left FFG region of interest (ROI) independently using age, sex and scanning site as covariates. A B-spline basis expansion of the covariate vector was used to model nonlinear effects of age. Normative models were derived in an unbiased manner across the entire sample under tenfold cross-validation<sup>37,49,99</sup>. To estimate voxel-wise/time point-wise deviations for each modality in each individual, we derived normative probability maps that quantify the deviation from the normative model summarized in *Z*-scores. These subject-specific *Z*-score images provide a statistical estimate of how much each individual’s recorded value differs from the predicted value at each voxel/time point. The accuracy of the normative model was evaluated using the correlation between the recorded and the predicted voxel values ( $\rho$ ), mean standardized log loss, standardized mean squared error and the EV (Supplementary Fig. 1) as well as based on the forward models (Extended Data Fig. 1). Furthermore, we compared model performance when modeling age linearly (without a B-spline basis expansion; Supplementary Fig. 2). To assess whether autistic and NAI differed in their extreme deviations based on unimodal features, thresholded *Z*-scores ( $Z > |2.6|$  (refs. 21,37,100), corresponding to the 99.5th percentile) were compared between the two groups using a two-sample *t*-test (Supplementary Methods). Code is available at <https://github.com/amarquand/PCNtoolkit>.

### LICA

To gain more comprehensive insights into cross-modal signatures of face processing, we merged the different individual-level deviations from all imaging modalities (GM volume, FFA connectivity, T-maps contrasting the faces to the shapes condition and the principal components of the source-reconstructed time series) using LICA<sup>51</sup> (Supplementary Methods). This is a Bayesian extension of the single modality ICA model, which provides an automatic and simultaneous decomposition of the brain features into ICs that characterize the intersubject brain variability. These multiple decompositions share a mixing matrix (that is, subject course) across individual feature factorizations that reflect the subject contributions to each IC. Here, LICA was used to merge the unthresholded *Z*-deviation maps derived from normative modeling across the four different imaging modalities within the right and left FFG ROIs. Each measure per hemisphere was treated separately resulting in eight input maps (that is, modalities). Hemispheres were modeled separately given known brain asymmetric differences in autism<sup>21,34</sup> and to study the hemispheric contributions and model the different noise characteristics individually. We estimated 50 ICs on the basis of our sample size and following recommendations described in earlier papers<sup>37,41,42,53</sup> (that is, sample size  $\sim N/4$ ). To evaluate the robustness of our selected model order ( $N = 50$ ), we reran LICA using different dimensional factorizations of subject loadings ( $N = 40$  and  $N = 60$ ) and computed correlations among them.

### Group differences

The subject loadings of all ICs were compared between autistic and NAI using a two-sample *t*-test. Normality and equal variances of subject loadings across the groups were formally tested using the

Kolmogorov–Smirnov test and Levene’s test, respectively (Supplementary Table 15). Multiple comparisons were corrected for using the FDR<sup>101</sup>. ICs showing significant group differences were further characterized by plotting each contributing modality’s spatial map and temporal profile (*Z* thresholded at the 95th percentile). To further characterize the most implicated regions within the FFG per modality, we computed the overlap between suprathreshold voxels and a structural (that is, the HOA, which covers the entire FFG) and a functional atlas (that is, a probabilistic functional atlas of the occipito-temporal cortex<sup>9</sup>, which covers category-specific FFG patches) (Supplementary Methods).

### Multimodal components

Next, given the current work’s focus on multimodal neural sources, we tested the hypothesis that multimodal components performed superior to unimodal components in differentiating autistic from NAI. For this, we calculated a MMI per IC to quantify the multimodal nature of modalities in each IC<sup>42</sup> (Supplementary Methods). The MMI ranges from 0 (equating to 100% unimodal contribution) to 1 (equating to equal contributions from all modalities). Multimodal components were defined as each single imaging modality (that is, regardless of hemisphere) not having more than a 90% contribution to each component and a MMI below 0.1 (Supplementary Fig. 4). Components below this threshold were treated as unimodal.

### Autism classification

Next, we implemented two SVM classifiers with a linear kernel—one using unimodal and one using multimodal components as features to test for the added value of multimodal features. The SVM was trained and evaluated using tenfold cross-validation. Class weighting was used to account for group size imbalance. The AUC was used as the performance metric to assess the classifier’s discrimination ability. To test for significant differences in AUC between multimodal and unimodal components, we generated a null distribution of AUC differences by shuffling the cross-validated scores 10,000 times and re-evaluating the classifier performance and computed the likelihood of observing the observed AUC difference under the null hypothesis. To test for robustness of the results, we reran analyses across different thresholds resulting in slightly varying degrees of multimodality ranging between 85% and 99% of single modality contributions. Given that each threshold resulted in a different number of unimodal versus multimodal components, we further checked whether results remained stable when forcing uni- and multimodal components to have the same number of features (Supplementary Methods).

### Clinical–cognitive associations

To test for the clinical relevance of multimodal ICs, we ran CCA<sup>102</sup> modeling the multivariate relationship between multimodal ICs and cognitive, clinical features related to either (1) social–communicative features related to social functioning and face processing in autism or (2) nonsocial features associated with autism. The statistical significance of the CCA modes was assessed by a complete permutation inference algorithm<sup>103</sup>, where both brain and behavior data were permuted separately across all participants with 10,000 iterations (Supplementary Methods). To visualize the spatial and temporal patterns of each imaging modality associated with each clinical cognitive measure, we computed the correlations between the original imaging data (that is, the *Z*-deviation maps) and the canonical imaging variate derived from the CCA<sup>104</sup>. Significance of correlation maps was assessed with 1,000 permutations, and significant clusters or time points were next visualized and characterized in terms of their functional and anatomical overlap with the VIS atlas<sup>9</sup> (Fig. 3f) and the HOA (Fig. 3k and Supplementary Methods). To assess the robustness of CCA results, we set a range of multimodal thresholds between 85% and 99% and selected ICs with modality contributions exceeding this threshold. We then

reran the CCA for each threshold to assess stability of results across varying degrees of multimodality.

### Reporting summary

Further information on research design is available in the Nature Portfolio Reporting Summary linked to this article.

### Data availability

LEAP data are shared through an application process codesigned with autistic people that preserves security and privacy—contact the corresponding author (D.L.F., Dorothea.floris@uzh.ch) for further details and application forms. Scripts used to implement the experimental task are covered by a material transfer agreement, which can be obtained through the corresponding author. The VIS atlas is available under <https://download.brainvoyager.com/data/visfAtlas.zip>. The HOA is distributed with fsl (<http://www.fmrib.ox.ac.uk/fsl/>), for further information see [https://ftp.nmr.mgh.harvard.edu/pub/dist/freesurfer/tutorial\\_packages/centos6/fsl\\_507/doc/wiki/Atlases.html](https://ftp.nmr.mgh.harvard.edu/pub/dist/freesurfer/tutorial_packages/centos6/fsl_507/doc/wiki/Atlases.html). Source data are provided with this paper.

### Code availability

Normative modeling code is available at <https://github.com/amarquand/PCNtoolkit>. LICA code is available at [https://github.com/allera/Llera\\_elife\\_2019\\_1/tree/master/matlab\\_flica\\_toolbox](https://github.com/allera/Llera_elife_2019_1/tree/master/matlab_flica_toolbox). CCA code is available at <https://github.com/andersonwinkler/PermCCA>.

### References

- Maenner, M. J. et al. Prevalence and characteristics of autism spectrum disorder among children aged 8 years—autism and developmental disabilities monitoring network, 11 sites, United States, 2018. *MMWR Surveill. Summ.* **70**, 1–16 (2021).
- Kanne, S. M. et al. The role of adaptive behavior in autism spectrum disorders: implications for functional outcome. *J. Autism Dev. Disord.* **41**, 1007–1018 (2011).
- Dawson, G., Webb, S. J. & McPartland, J. Understanding the nature of face processing impairment in autism: insights from behavioral and electrophysiological studies. *Dev. Neuropsychol.* **27**, 403–424 (2005).
- Sasson, N. J. The development of face processing in autism. *J. Autism Dev. Disord.* **36**, 381–394 (2006).
- Meyer-Lindenberg, H. et al. Facial expression recognition is linked to clinical and neurofunctional differences in autism. *Mol. Autism* **13**, 43 (2022).
- Chevallier, C., Hugué, P., Happé, F., George, N. & Conty, L. Salient social cues are prioritized in autism spectrum disorders despite overall decrease in social attention. *J. Autism Dev. Disord.* **43**, 1642–1651 (2013).
- Schultz, R. T. Developmental deficits in social perception in autism: the role of the amygdala and fusiform face area. *Int. J. Dev. Neurosci.* **23**, 125–141 (2005).
- Sui, J., Adali, T., Yu, Q., Chen, J. & Calhoun, V. D. A review of multivariate methods for multimodal fusion of brain imaging data. *J. Neurosci. Methods* **204**, 68–81 (2012).
- Rosenke, M., van Hoof, R., van den Hurk, J., Grill-Spector, K. & Goebel, R. A probabilistic functional atlas of human occipitotemporal visual cortex. *Cereb. Cortex* **31**, 603–619 (2021).
- Zhang, W. et al. Functional organization of the fusiform gyrus revealed with connectivity profiles. *Hum. Brain Mapp.* **37**, 3003–3016 (2016).
- Gauthier, I. et al. The fusiform ‘face area’ is part of a network that processes faces at the individual level. *J. Cogn. Neurosci.* <https://doi.org/10.1162/089892900562165> (2000).
- Taylor, J. C., Wiggett, A. J. & Downing, P. E. Functional MRI analysis of body and body part representations in the extrastriate and fusiform body areas. *J. Neurophysiol.* **98**, 1626–1633 (2007).
- Wang, X. et al. Where color rests: spontaneous brain activity of bilateral fusiform and lingual regions predicts object color knowledge performance. *Neuroimage* **76**, 252–263 (2013).
- McCarthy, G., Puce, A., Gore, J. C. & Allison, T. Face-specific processing in the human fusiform gyrus. *J. Cogn. Neurosci.* **9**, 605–610 (1997).
- Kanwisher, N. & Yovel, G. The fusiform face area: a cortical region specialized for the perception of faces. *Philos. Trans. R. Soc. B* **361**, 2109–2128 (2006).
- Bentin, S., Allison, T., Puce, A., Perez, E. & McCarthy, G. Electrophysiological studies of face perception in humans. *J. Cogn. Neurosci.* **8**, 551–565 (1996).
- Bötzel, K., Schulze, S. & Stodieck, S. R. Scalp topography and analysis of intracranial sources of face-evoked potentials. *Exp. Brain Res.* **104**, 135–143 (1995).
- Rossion, B. et al. Hemispheric asymmetries for whole-based and part-based face processing in the human fusiform gyrus. *J. Cogn. Neurosci.* **12**, 793–802 (2000).
- Yovel, G., Tambini, A. & Brandman, T. The asymmetry of the fusiform face area is a stable individual characteristic that underlies the left-visual-field superiority for faces. *Neuropsychologia* **46**, 3061–3068 (2008).
- Cardinale, R. C., Shih, P., Fishman, I., Ford, L. M. & Müller, R. A. Pervasive rightward asymmetry shifts of functional networks in autism spectrum disorder. *JAMA Psychiatry* <https://doi.org/10.1001/jamapsychiatry.2013.382> (2013).
- Floris, D. L. et al. Atypical brain asymmetry in autism—a candidate for clinically meaningful stratification. *Biol. Psychiatry Cogn. Neurosci. Neuroimag.* **6**, 802–812 (2021).
- Nickl-Jockschat, T. et al. Neural networks related to dysfunctional face processing in autism spectrum disorder. *Brain Struct. Funct.* **220**, 2355–2371 (2015).
- Pierce, K., Haist, F., Sedaghat, F. & Courchesne, E. The brain response to personally familiar faces in autism: findings of fusiform activity and beyond. *Brain* **127**, 2703–2716 (2004).
- Kleinmans, N. M. et al. Abnormal functional connectivity in autism spectrum disorders during face processing. *Brain* **131**, 1000–1012 (2008).
- Koshino, H. et al. fMRI investigation of working memory for faces in autism: visual coding and underconnectivity with frontal areas. *Cereb. Cortex* **18**, 289–300 (2008).
- Kang, E. et al. Atypicality of the N170 event-related potential in autism spectrum disorder: a meta-analysis. *Biol. Psychiatry Cogn. Neurosci. Neuroimag.* **3**, 657–666 (2018).
- Mason, L. et al. Stratifying the autistic phenotype using electrophysiological indices of social perception. *Sci. Transl. Med.* **14**, eabf8987 (2022).
- Waiter, G. D. et al. A voxel-based investigation of brain structure in male adolescents with autistic spectrum disorder. *Neuroimage* **22**, 619–625 (2004).
- Van Kooten, I. A. J. et al. Neurons in the fusiform gyrus are fewer and smaller in autism. *Brain* **131**, 987–999 (2008).
- Herbert, M. R. et al. Abnormal asymmetry in language association cortex in autism. *Ann. Neurol.* **52**, 588–596 (2002).
- Neuhäus, E. et al. The relationship between early neural responses to emotional faces at age 3 and later autism and anxiety symptoms in adolescents with autism. *J. Autism Dev. Disord.* **46**, 2450–2463 (2016).
- Webb, S. J. et al. Developmental change in the ERP responses to familiar faces in toddlers with autism spectrum disorders versus typical development. *Child Dev.* **82**, 1868–1886 (2011).
- Gao, C., Conte, S., Richards, J. E., Xie, W. & Hanayik, T. The neural sources of N170: understanding timing of activation in face-selective areas. *Psychophysiology* **56**, e13336 (2019).



34. Dougherty, C. C., Evans, D. W., Katuwal, G. J. & Michael, A. M. Asymmetry of fusiform structure in autism spectrum disorder: trajectory and association with symptom severity. *Mol. Autism* **7**, 28 (2016).
35. Iidaka, T., Matsumoto, A., Haneda, K., Okada, T. & Sadato, N. Hemodynamic and electrophysiological relationship involved in human face processing: evidence from a combined fMRI-ERP study. *Brain and Cognition* **60**, 176–186 (2006).
36. Puce, A. et al. The human temporal lobe integrates facial form and motion: evidence from fMRI and ERP studies. *Neuroimage* **19**, 861–869 (2003).
37. Holz, N. E. et al. Age-related brain deviations and aggression. *Psychol. Med.* <https://doi.org/10.1017/S003329172200068X> (2022).
38. Brown, T. T. et al. Neuroanatomical assessment of biological maturity. *Curr. Biol.* **22**, 1693–1698 (2012).
39. Erus, G. et al. Imaging patterns of brain development and their relationship to cognition. *Cereb. Cortex* **25**, 179–188 (2015).
40. Liem, F. et al. Predicting brain-age from multimodal imaging data captures cognitive impairment. *Neuroimage* **148**, 179–188 (2017).
41. Mei, T. et al. Autism is associated with interindividual variations of gray and white matter morphology. *Biol. Psychiatry Cogn. Neurosci. Neuroimaging* <https://doi.org/10.1016/j.bpsc.2022.08.011> (2022).
42. Francx, W. et al. Integrated analysis of gray and white matter alterations in attention-deficit/hyperactivity disorder. *Neuroimage Clin.* **11**, 357–367 (2016).
43. Achalia, R. et al. A proof of concept machine learning analysis using multimodal neuroimaging and neurocognitive measures as predictive biomarker in bipolar disorder. *Asian J. Psychiatr.* **50**, 101984 (2020).
44. Kim, J. I. et al. Classification of preschoolers with low-functioning autism spectrum disorder using multimodal MRI data. *J. Autism Dev. Disord.* **53**, 25–37 (2023).
45. Sui, J. et al. Combination of FMRI-SMRI-EEG data improves discrimination of schizophrenia patients by ensemble feature selection. *Annu. Int. Conf. IEEE Eng. Med. Biol. Soc.* **2014**, 3889–3892 (2014).
46. Oblong, L. M. et al. Linking functional and structural brain organisation with behaviour in autism: a multimodal EU-AIMS Longitudinal European Autism Project (LEAP) study. *Mol. Autism* **14**, 32 (2023).
47. Charman, T. et al. The EU-AIMS Longitudinal European Autism Project (LEAP): clinical characterisation. *Mol. Autism* **8**, 27 (2017).
48. Loth, E. et al. The EU-AIMS Longitudinal European Autism Project (LEAP): design and methodologies to identify and validate stratification biomarkers for autism spectrum disorders. *Mol. Autism* **8**, 24 (2017).
49. Marquand, A. F., Rezek, I., Buitelaar, J. & Beckmann, C. F. Understanding heterogeneity in clinical cohorts using normative models: beyond case-control studies. *Biol. Psychiatry* **80**, 552–561 (2016).
50. Parkes, L. et al. Transdiagnostic dimensions of psychopathology explain individuals' unique deviations from normative neurodevelopment in brain structure. *Transl. Psychiatry* **11**, 232 (2021).
51. Groves, A. R., Beckmann, C. F., Smith, S. M. & Woolrich, M. W. Linked independent component analysis for multimodal data fusion. *Neuroimage* **54**, 2198–2217 (2011).
52. Rutherford, S. et al. Evidence for embracing normative modeling. *eLife* **12**, e85082 (2023).
53. Llera, A., Wolfers, T., Mulders, P. & Beckmann, C. F. Inter-individual differences in human brain structure and morphology link to variation in demographics and behavior. *eLife* **8**, e44443 (2019).
54. Hus, V. & Lord, C. The autism diagnostic observation schedule, module 4: revised algorithm and standardized severity scores. *J. Autism Dev. Dis.* **44**, 1996–2012 (2014).
55. Lord, C., Rutter, M. & Le Couteur, A. Autism diagnostic interview-revised: a revised version of a diagnostic interview for caregivers of individuals with possible pervasive developmental disorders. *J. Autism Dev. Dis.* **24**, 659–685 (1994).
56. Sparrow, S. S., Cicchetti, D. V. & Balla, D. A. *Vineland Adaptive Behavior Scales* 2nd edn (American Guidance Service, 2005).
57. Baron-Cohen, S., Wheelwright, S., Hill, J., Raste, Y. & Plumb, I. The 'reading the mind in the eyes' test revised version: a study with normal adults, and adults with Asperger syndrome or high-functioning autism. *J. Child Psychol. Psychiatry* **42**, 241–251 (2001).
58. Hariri, A. R., Tessitore, A., Mattay, V. S., Fera, F. & Weinberger, D. R. The amygdala response to emotional stimuli: a comparison of faces and scenes. *Neuroimage* **17**, 317–323 (2002).
59. Hariri, A. R. et al. Dextroamphetamine modulates the response of the human amygdala. *Neuropsychopharmacology* **27**, 1036–1040 (2002).
60. Hariri, A. R. et al. Serotonin transporter genetic variation and the response of the human amygdala. *Science* **297**, 400–403 (2002).
61. Bodfish, J. W., Symons, F. J., Parker, D. E. & Lewis, M. H. *Repetitive Behavior Scale-Revised* (APA PsycNet, 2000).
62. Auyeung, B. et al. The children's empathy quotient and systemizing quotient: sex differences in typical development and in autism spectrum conditions. *J. Autism Dev. Dis.* **39**, 1509–1521 (2009).
63. Auyeung, B., Allison, C., Wheelwright, S. & Baron-Cohen, S. Brief report: development of the adolescent empathy and systemizing quotients. *J. Autism Dev. Dis.* **42**, 2225–2235 (2012).
64. Baron-Cohen, S., Richler, J., Bisarya, D., Gurunathan, N. & Wheelwright, S. The systemizing quotient: an investigation of adults with Asperger syndrome or high-functioning autism, and normal sex differences. *Philos. Trans. R. Soc. B* **358**, 163–175 (2003).
65. Critchley, H. D. et al. The functional neuroanatomy of social behaviour: changes in cerebral blood flow when people with autistic disorder process facial expressions. *Brain* **123**, 2203–2212 (2000).
66. Corbett, B. A. et al. A functional and structural study of emotion and face processing in children with autism. *Psychiatry Res. Neuroimaging* **173**, 196–205 (2009).
67. Lynn, A. C. et al. Functional connectivity differences in autism during face and car recognition: underconnectivity and atypical age-related changes. *Dev. Sci.* **21**, e12508 (2018).
68. Bentin, S. & Deouell, L. Y. Structural encoding and identification in face processing: erp evidence for separate mechanisms. *Cogn. Neuropsychol.* **17**, 35–55 (2000).
69. Chevallier, C., Kohls, G., Troiani, V., Brodtkin, E. S. & Schultz, R. T. The social motivation theory of autism. *Trends Cogn. Sci.* **16**, 231–239 (2012).
70. Pitcher, D., Walsh, V. & Duchaine, B. The role of the occipital face area in the cortical face perception network. *Exp. Brain Res.* **209**, 481–493 (2011).
71. Happé, F. & Frith, U. The weak coherence account: detail-focused cognitive style in autism spectrum disorders. *J. Autism Dev. Dis.* **36**, 5–25 (2006).
72. Watson, T. L. Implications of holistic face processing in autism and schizophrenia. *Front. Psychol.* **4**, 414 (2013).
73. Schultz, R. T. et al. Abnormal ventral temporal cortical activity during face discrimination among individuals with autism and Asperger syndrome. *Arc. Gen. Psychiatry* **57**, 331–340 (2000).
74. Pierce, K., Müller, R. A., Ambrose, J., Allen, G. & Courchesne, E. Face processing occurs outside the fusiform 'face area' in autism: evidence from functional MRI. *Brain* **124**, 2059–2073 (2001).



75. Schweinberger, S. R., Pickering, E. C., Jentsch, I., Burton, A. M. & Kaufmann, J. M. Event-related brain potential evidence for a response of inferior temporal cortex to familiar face repetitions. *Cogn. Brain Res.* **14**, 398–409 (2002).
76. Schweinberger, S. R., Huddy, V. & Burton, A. M. N25Or: a face-selective brain response to stimulus repetitions. *Neuroreport* **15**, 1501–1505 (2004).
77. Morgan, H. M., Klein, C., Boehm, S. G., Shapiro, K. L. & Linden, D. E. J. Working memory load for faces modulates P300, N170, and N25Or. *J. Cogn. Neurosci.* **20**, 989–1002 (2008).
78. Groves, A. R. et al. Benefits of multi-modal fusion analysis on a large-scale dataset: life-span patterns of inter-subject variability in cortical morphometry and white matter microstructure. *Neuroimage* **63**, 365–380 (2012).
79. Caspers, J. et al. Functional characterization and differential coactivation patterns of two cytoarchitectonic visual areas on the human posterior fusiform gyrus. *Hum. Brain Mapp.* **35**, 2754–2767 (2014).
80. Floris, D. L. et al. Atypically rightward cerebral asymmetry in male adults with autism stratifies individuals with and without language delay. *Hum. Brain Mapp.* **37**, 230–253 (2016).
81. Calhoun, V. D. & Sui, J. Multimodal fusion of brain imaging data: a key to finding the missing link(s) in complex mental illness. *Biol. Psychiatry* **1**, 230–244 (2016).
82. Aoki, Y., Cortese, S. & Tansella, M. Neural bases of atypical emotional face processing in autism: a meta-analysis of fMRI studies. *World J. Biol. Psychiatry* **16**, 291–300 (2015).
83. Haxby, J. V., Hoffman, E. A. & Gobbini, M. I. The distributed human neural system for face perception. *Trends Cogn. Sci.* **4**, 223–233 (2000).
84. Rossion, B. et al. A network of occipito-temporal face-sensitive areas besides the right middle fusiform gyrus is necessary for normal face processing. *Brain* <https://doi.org/10.1093/brain/awg241> (2003).
85. Barton, J. J. S., Press, D. Z., Keenan, J. P. & O'Connor, M. Lesions of the fusiform face area impair perception of facial configuration in prosopagnosia. *Neurology* **58**, 71–78 (2002).
86. Floris, D. L. et al. The link between autism and sex-related neuroanatomy, and associated cognition and gene expression. *Am. J. Psychiatry* **180**, 50–64 (2023).
87. Bukowski, H., Dricot, L., Hanseeuw, B. & Rossion, B. Cerebral lateralization of face-sensitive areas in left-handers: only the FFA does not get it right. *Cortex* **49**, 2583–2589 (2013).
88. Frässle, S., Krach, S., Paulus, F. M. & Jansen, A. Handedness is related to neural mechanisms underlying hemispheric lateralization of face processing. *Sci. Rep.* **6**, 27153 (2016).
89. Berman, M. G. et al. Evaluating functional localizers: the case of the FFA. *Neuroimage* **50**, 56–71 (2010).
90. Fox, C. J., Iaria, G. & Barton, J. J. S. Defining the face processing network: optimization of the functional localizer in fMRI. *Hum. Brain Mapp.* **30**, 1637–1651 (2009).
91. Jones, W. et al. Development and replication of objective measurements of social visual engagement to aid in early diagnosis and assessment of autism. *JAMA Netw. Open* **6**, e2330145 (2023).
92. Jones, W. & Klin, A. Attention to eyes is present but in decline in 2–6-month-old infants later diagnosed with autism. *Nature* **504**, 427–431 (2013).
93. Lord, C. et al. The autism diagnostic observation schedule–generic: a standard measure of social and communication deficits associated with the spectrum of autism. *J. Autism Dev. Dis.* **30**, 205–223 (2000).
94. Lord, C. et al. *Autism Diagnostic Observation Schedule (ADOS-2) 2nd edn (part I): modules 1–4* (Western Psychological Service, 2012).
95. Llera, A. et al. Evaluation of data imputation strategies in complex, deeply-phenotyped data sets: the case of the EU–AIMS Longitudinal European Autism Project. *BMC Med. Res. Methodol.* **22**, 229 (2022).
96. Looden, T. et al. Patterns of connectome variability in autism across five functional activation tasks: findings from the LEAP project. *Mol. Autism* **13**, 53 (2022).
97. Marquand, A. F. et al. Conceptualizing mental disorders as deviations from normative functioning. *Mol. Psychiatry* **24**, 1415–1424 (2019).
98. Fraza, C. J., Dinga, R., Beckmann, C. F. & Marquand, A. F. Warped Bayesian linear regression for normative modelling of big data. *Neuroimage* **245**, 118715 (2021).
99. Holz, N. E. et al. A stable and replicable neural signature of lifespan adversity in the adult brain. *Nat. Neurosci.* <https://doi.org/10.1038/s41593-023-01410-8> (2023).
100. Wolfers, T. et al. Mapping the heterogeneous phenotype of schizophrenia and bipolar disorder using normative models. *JAMA Psychiatry* **75**, 1146–1155 (2018).
101. Benjamini, Y. & Hochberg, Y. On the adaptive control of the false discovery rate in multiple testing with independent statistics. *J. Educ. Behav. Stat.* <https://doi.org/10.3102/10769986025001060> (2000).
102. Hotelling, H. Relations between two sets of variates. *Biometrika* **28**, 321–377 (1936).
103. Winkler, A. M., Renaud, O., Smith, S. M. & Nichols, T. E. Permutation inference for canonical correlation analysis. *Neuroimage* **220**, 117065 (2020).
104. Ball, G. et al. Multimodal image analysis of clinical influences on preterm brain development. *Ann. Neurol.* **82**, 233–246 (2017).

## Acknowledgments

We thank all participants and their families for participating in the studies that contribute to the datasets used in this research. We also gratefully acknowledge the contributions of all members of the EU–AIMS/AIMS-2-TRIALS LEAP group: J. Ahmad, S. Ambrosino, B. Auyeung, S. Baumeister, S. Bölte, C. Bours, M. Brammer, D. Brandeis, C. Brogna, Y. de Bruijn, B. Chakrabarti, I. Cornelissen, D. Crawley, G. Dumas, J. Faulkner, V. Frouin, P. Garcés, D. Goyard, L. Ham, H. Hayward, J. Hipp, M.H. Johnson, E.J.H. Jones, X. Liogier D'ardhuy, D.J. Lythgoe, R. Mandl, L. Mason, A. Meyer-Lindenberg, N. Mueller, B. Oakley, L. O'Dwyer, B. Oranje, G. Pandina, A.M. Persico, B. Ruggeri, A. Ruigrok, J. Sabet, R. Sacco, A. San J. Cáceres, E. Simonoff, W. Spooren, R. Toro, H. Tost, J. Waldman, S.C.R. Williams, C. Wooldridge and M.P. Zwiers. This project has received funding from the Innovative Medicines Initiative 2 Joint Undertaking under grant agreement no. 115300 (for EU–AIMS) and no. 777394 (for AIMS-2-TRIALS). This Joint Undertaking receives support from the European Union's Horizon 2020 research and innovation program and EFPIA and AUTISM SPEAKS, Autistica, SFARI. Any views expressed are those of the author(s) and not necessarily those of the funders (IHI-JU2). This work was also supported by the Netherlands Organization for Scientific Research through grants (grant no. 864.12.003 to C.F.B.); from the FP7 (grant no. 602805, AGGRESSOTYPE to J.K.B.), 603016 (MATRICS) and 278948 (TACTICS); and from the European Community's Horizon 2020 Program (H2020/2014-2020) (grant nos. 643051 (MiND) and 642996 (BRAINVIEW)). This work received funding from the Wellcome Trust UK Strategic Award (award no. 098369/Z/12/Z) and from the National Institute for Health Research Maudsley Biomedical Research Center (to D.G.M.M.). D.L.F. is supported by the UZH Postdoc Grant (grant no. FK-23-085) and received funding from the European Union's Horizon 2020 research and innovation program under the Marie Skłodowska-Curie grant agreement no 101025785. E.J.H.J. and R.H. received funding from SFARI GAIINS (grant no. 10039678). N.E.H. was supported by the German Research Foundation (grant no. GRK2350/1)

and the German Center for Mental Health. S.B.-C. received funding from the Wellcome Trust 214322\Z\18\Z, the Autism Center of Excellence at Cambridge, SFARI, the Templeton World Charitable Fund, the MRC and the NIHR Cambridge Biomedical Research Center. B.H.V. is supported by the Swiss National Science Foundation (10001C\_197480) and the UZH Postdoc Grant (grant no. FK-23-086). N.L. is supported by Swiss National Foundation (10001C\_220048). C.F.B. gratefully acknowledges funding from the Wellcome Trust Collaborative Award in Science 215573/Z/19/Z and the Netherlands Organization for Scientific Research Vici Grant (grant no. 17854). This work has also been supported by the Horizon 2020 Program (grant no. 847818 (CANDY)). The funders had no role in the design of the study; in the collection, analyses, or interpretation of data; in the writing of the manuscript, or in the decision to publish the results.

## Author contributions

D.L.F. carried out the study design, data preprocessing and analysis and wrote the paper. A.L., T.M., B.H.V. and N.J.F. carried out supervision and advised on LICA and interpretation. M.Z., N.E.H. and C.E. carried out supervision and advised on normative modeling analysis and interpretation. C.M. and S.B. carried out fMRI preprocessing. E.J.H.J., L.M. and R.H. carried out EEG data preprocessing. C.M.P. carried out analysis direction and interpretation. T.C. carried out the clinical/design of study and interpreted the results. F.D.A., S.D., T. Banaschewski, C.E., R.J.H., S.B.-C., T. Bourgeron, E.L., D.G.M.M., J.K.B. and C.F.B. secured funding and supervised the overall study and analysis direction and interpretation of results. N.L. carried out the study design and supervision of the overall analytic strategy. All authors revised the manuscript for intellectual content.

## Competing interests

J.K.B. has been a consultant to, advisory board member of and a speaker for Takeda/Shire, Medice, Roche and Servier. He is not an employee of any of these companies and not a stock shareholder of any of these companies. He has no other financial or material support, including expert testimony, patents, or royalties. C.F.B. is director and shareholder in SBGneuro Ltd. T.C. has received consultancy fees from Roche and Servier and received book royalties from Guildford Press and Sage. T. Banaschewski served in an advisory or consultancy role for ADHS digital, Infectopharm, Lundbeck, Medice, Neurim Pharmaceuticals, Oberberg GmbH, Roche and Takeda. He received conference support or speaker's fees from Medice and Takeda.

He received royalties from Hogrefe, Kohlhammer, CIP Medien and Oxford University Press; the present work is unrelated to these relationships. The other authors declare no competing interests.

## Additional information

**Extended data** is available for this paper at <https://doi.org/10.1038/s44220-024-00349-4>.

**Supplementary information** The online version contains supplementary material available at <https://doi.org/10.1038/s44220-024-00349-4>.

**Correspondence and requests for materials** should be addressed to Dorothea L. Floris.





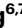
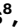















**Peer review information** *Nature Mental Health* thanks Jason W. Griffin and the other, anonymous reviewer(s) for their contribution to the peer review of this work.

**Reprints and permissions information** is available at [www.nature.com/reprints](http://www.nature.com/reprints).

**Publisher's note** Springer Nature remains neutral with regard to jurisdictional claims in published maps and institutional affiliations.

**Open Access** This article is licensed under a Creative Commons Attribution-NonCommercial-NoDerivatives 4.0 International License, which permits any non-commercial use, sharing, distribution and reproduction in any medium or format, as long as you give appropriate credit to the original author(s) and the source, provide a link to the Creative Commons licence, and indicate if you modified the licensed material. You do not have permission under this licence to share adapted material derived from this article or parts of it. The images or other third party material in this article are included in the article's Creative Commons licence, unless indicated otherwise in a credit line to the material. If material is not included in the article's Creative Commons licence and your intended use is not permitted by statutory regulation or exceeds the permitted use, you will need to obtain permission directly from the copyright holder. To view a copy of this licence, visit <http://creativecommons.org/licenses/by-nc-nd/4.0/>.

© The Author(s) 2025

**Dorothea L. Floris** <sup>1,2,3</sup> , **Alberto Llera** <sup>2,3,4</sup>, **Mariam Zabih** <sup>2,5</sup>, **Carolin Moessnang** <sup>6,7</sup>, **Emily J. H. Jones** <sup>8</sup>, **Luke Mason** <sup>8,9</sup>, **Rianne Haartsen** <sup>8</sup>, **Nathalie E. Holz** <sup>10,11</sup>, **Ting Mei** <sup>2,3</sup>, **Camille Elleaume**<sup>1</sup>, **Bruno Hebling Vieira** <sup>1</sup>, **Charlotte M. Pretzsch** <sup>9</sup>, **Natalie J. Forde** <sup>2,3</sup>, **Sarah Baumeister** <sup>10</sup>, **Flavio Dell'Acqua** <sup>9,12</sup>, **Sarah Durston**<sup>13</sup>, **Tobias Banaschewski** <sup>10,11</sup>, **Christine Ecker**<sup>14</sup>, **Rosemary J. Holt**<sup>15</sup>, **Simon Baron-Cohen** <sup>15</sup>, **Thomas Bourgeron**<sup>16</sup>, **Tony Charman** <sup>17</sup>, **Eva Loth** <sup>9,12</sup>, **Declan G. M. Murphy** <sup>9,12</sup>, **Jan K. Buitelaar** <sup>2,3,18</sup>, **Christian F. Beckmann**<sup>2,3,19</sup>, **the EU-AIMS LEAP group\*** & **Nicolas Langer**<sup>1,20</sup>

<sup>1</sup>Methods of Plasticity Research, Department of Psychology, University of Zurich, Zurich, Switzerland. <sup>2</sup>Donders Institute for Brain, Cognition, and Behavior, Radboud University Nijmegen, Nijmegen, The Netherlands. <sup>3</sup>Department for Cognitive Neuroscience, Radboud University Medical Center, Nijmegen, The Netherlands. <sup>4</sup>Lis Data Solutions, Santander, Spain. <sup>5</sup>MRC Unit Lifelong Health and Aging, University College London, London, UK. <sup>6</sup>Department of Psychiatry and Psychotherapy, Central Institute of Mental Health, Medical Faculty Mannheim, University of Heidelberg, Mannheim, Germany. <sup>7</sup>Department of Applied Psychology, SRH University, Heidelberg, Germany. <sup>8</sup>Centre for Brain and Cognitive Development, Birkbeck, University of London, London, UK. <sup>9</sup>Department of Forensic and Neurodevelopmental Sciences, Institute of Psychiatry, Psychology and Neuroscience, King's College London, London, UK. <sup>10</sup>Department of Child and Adolescent Psychiatry, Central Institute of Mental Health, Medical Faculty Mannheim, University of Heidelberg, Mannheim, Germany. <sup>11</sup>German Center for Mental Health (DZPG), Partner site Mannheim-Heidelberg-Ulm, Mannheim, Germany. <sup>12</sup>Institute for Translational Neurodevelopment, Institute of Psychiatry, Psychology and Neuroscience, King's College London, London, UK. <sup>13</sup>Department of Psychiatry, Brain Center Rudolf Magnus, University Medical Center, Utrecht, The Netherlands. <sup>14</sup>Department of Child and Adolescent Psychiatry, University Hospital, Goethe University, Frankfurt am Main, Germany. <sup>15</sup>Autism Research Centre, Department of Psychiatry, University of Cambridge, Cambridge,

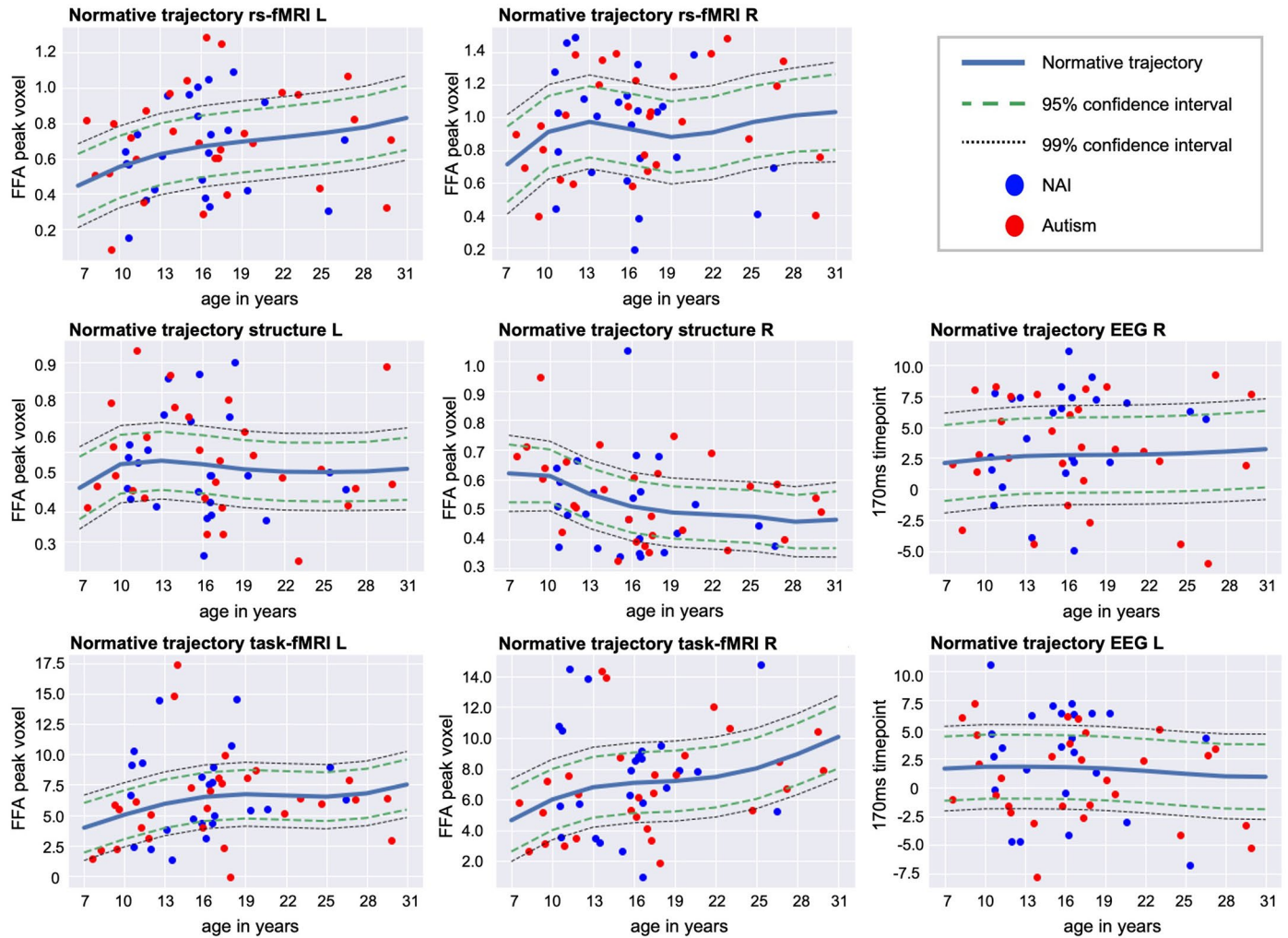
UK. <sup>16</sup>Human Genetics and Cognitive Functions Unity, Institut Pasteur, Paris, France. <sup>17</sup>Department of Psychology, Institute of Psychiatry, Psychology and Neuroscience, King's College London, London, UK. <sup>18</sup>Karakter Child and Adolescent Psychiatry University Centre, Nijmegen, The Netherlands. <sup>19</sup>Wellcome Centre for Integrative Neuroimaging, University of Oxford, Oxford, UK. <sup>20</sup>Neuroscience Center Zurich, Zurich, Switzerland.  
\*A list of authors and their affiliations appears at the end of the paper. ✉e-mail: [Dorothea.floris@uzh.ch](mailto:Dorothea.floris@uzh.ch)

---

**the EU-AIMS LEAP group**

---

**Dorothea L. Floris<sup>1,2,3</sup>, Alberto Llera<sup>2,3,4</sup>, Mariam Zabihi<sup>2,5</sup>, Carolin Moessnang<sup>6,7</sup>, Emily J. H. Jones<sup>8</sup>, Luke Mason<sup>8,9</sup>, Rianne Haartsen<sup>8</sup>, Nathalie E. Holz<sup>10,11</sup>, Ting Mei<sup>2,3</sup>, Charlotte M. Pretzsch<sup>9</sup>, Natalie J. Forde<sup>2,3</sup>, Sarah Baumeister<sup>10</sup>, Flavio Dell'Acqua<sup>9,12</sup>, Sarah Durston<sup>13</sup>, Tobias Banaschewski<sup>10,11</sup>, Christine Ecker<sup>14</sup>, Rosemary J. Holt<sup>15</sup>, Simon Baron-Cohen<sup>15</sup>, Thomas Bourgeron<sup>16</sup>, Tony Charman<sup>17</sup>, Eva Loth<sup>9,12</sup>, Declan G. M. Murphy<sup>9,12</sup>, Jan K. Buitelaar<sup>2,3,18</sup> & Christian F. Beckmann<sup>2,3,19</sup>**

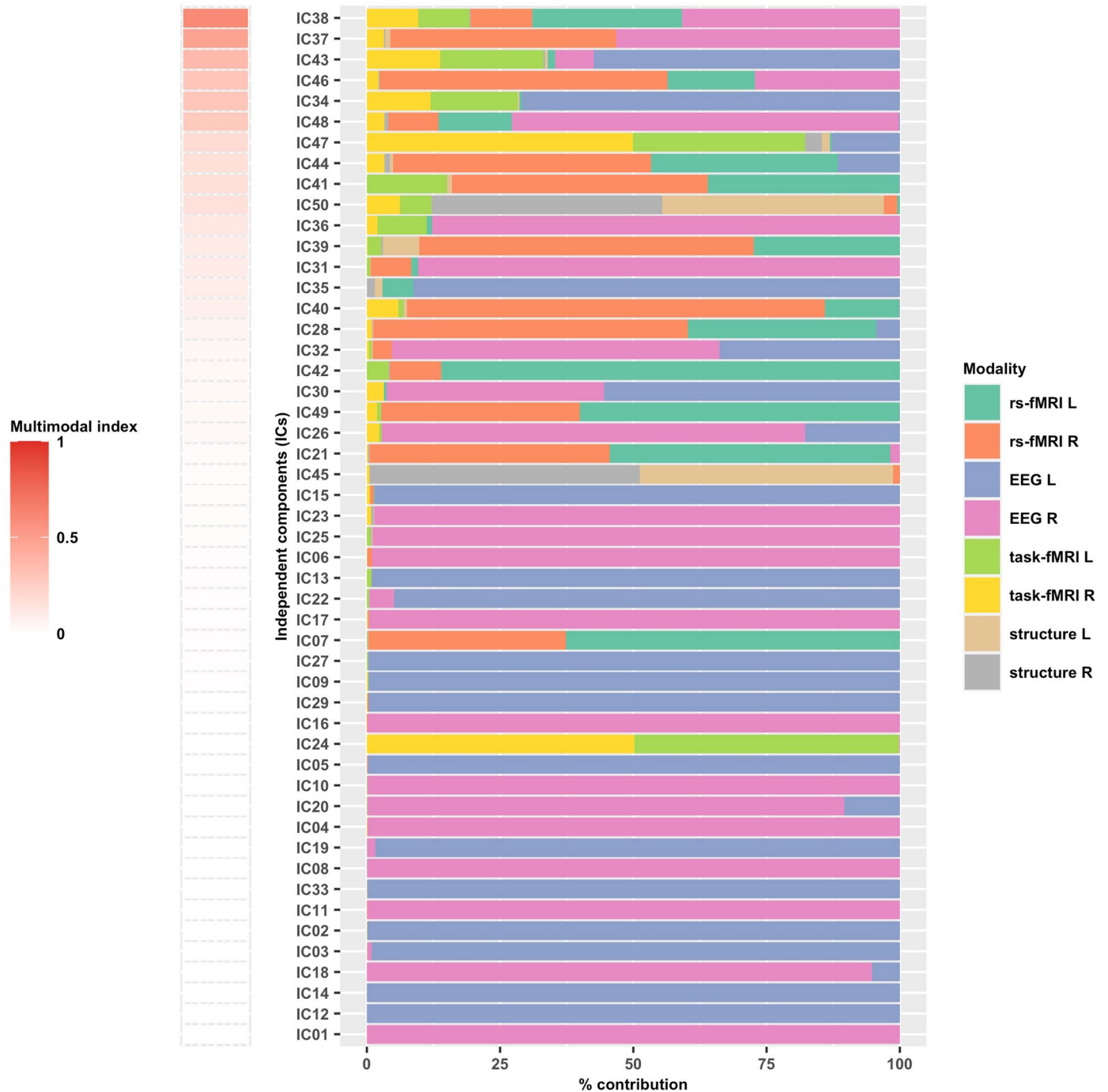


**Extended Data Fig. 1 | Example forward models across the modalities.**

Forward models are shown (estimated across all individuals) depicting the spatial and temporal representations of the voxel-wise/ timepoint-wise normative model for each imaging modality per hemisphere. For imaging modalities (structure, task-fMRI, resting-state fMRI) the normative model of the peak activation voxel within the fusiform face area (FFA) is shown, whereas for EEG at timepoint 170 ms. The regression line depicts the predicted values between 7 and

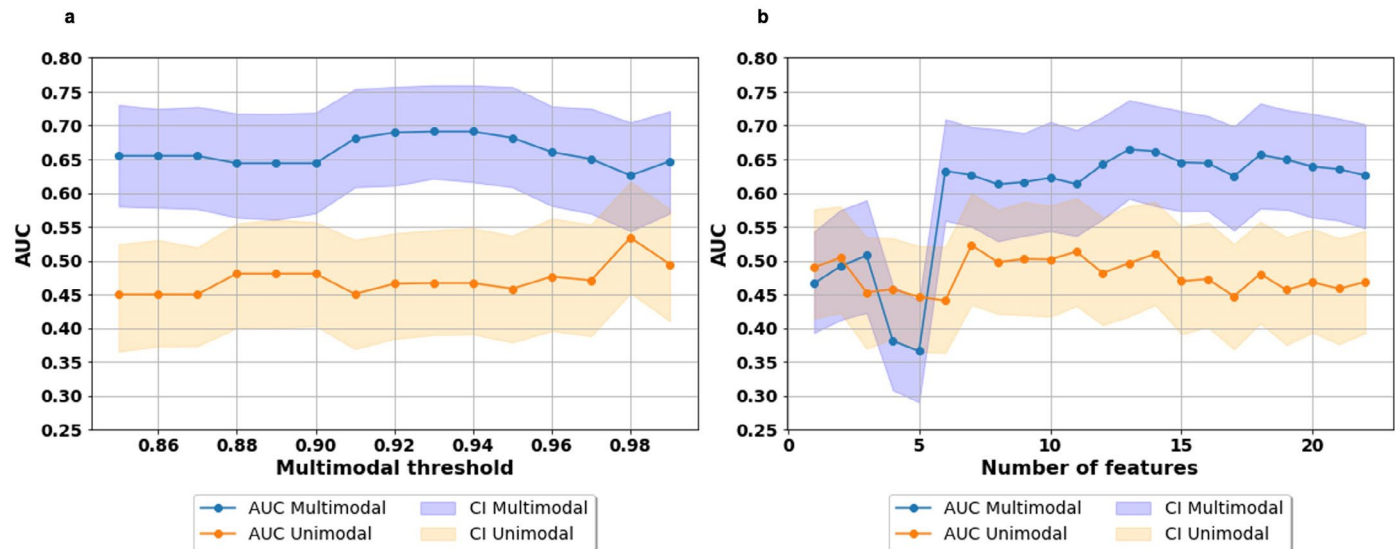
30 years of age along with centiles of confidence (95th and 99th). The blue dots are the true values for nonautistic males in the KCL site, whereas the red dots are the true values for the autistic males in the KCL site. Given that the categorical covariates (sex, site) will render slightly different slopes, here, we only plotted the trajectories in males and in the largest acquisition site (KCL) for descriptive purposes. **Abbreviations:** FFA=fusiform face area; NAI=nonautistic individuals; L=left; R=right.





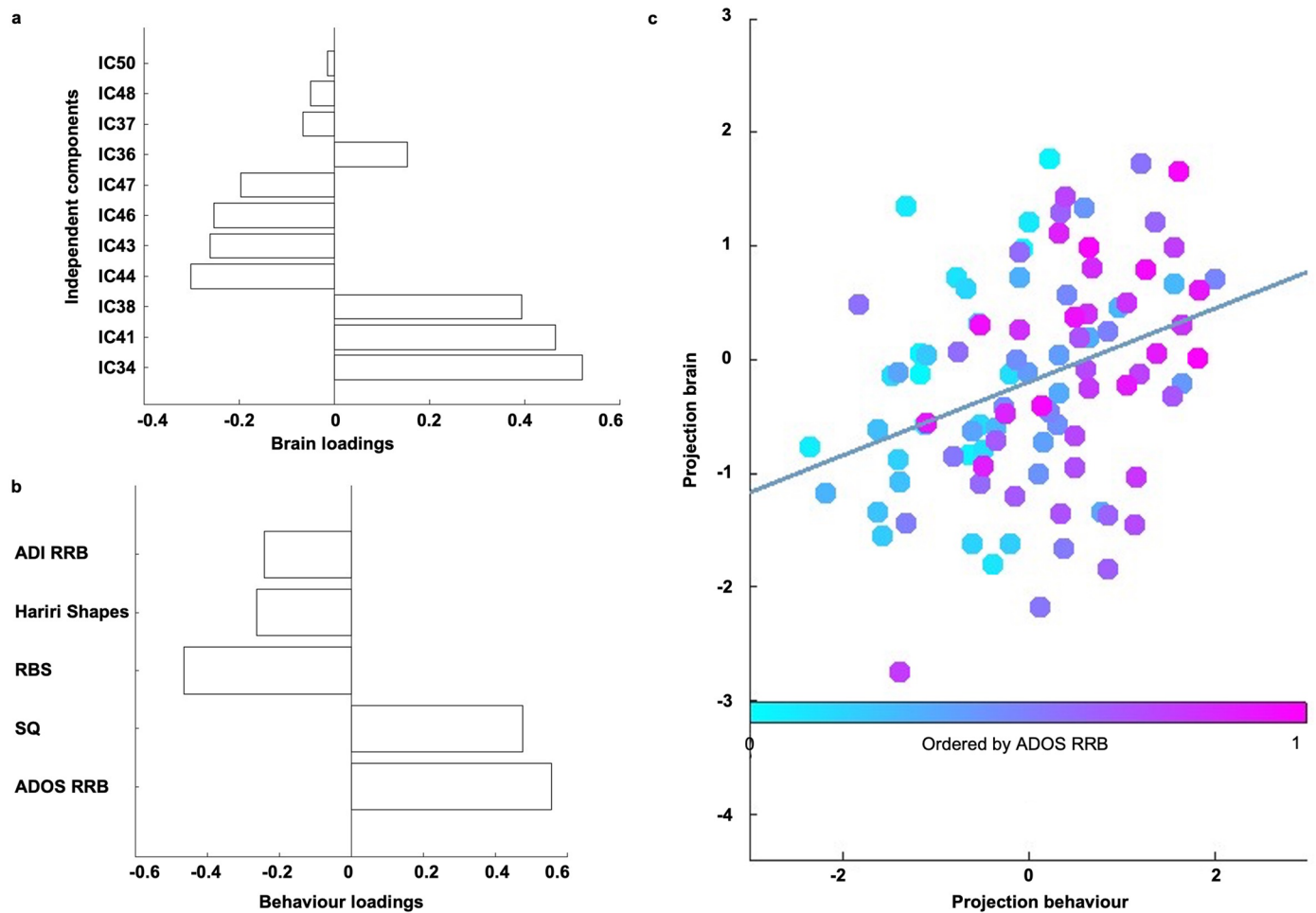
**Extended Data Fig. 2 | Fifty independent components.** We identified 50 independent components using Linked ICA. These are ordered according to how multimodal they are (that is, multimodal index). Each color represents one of the eight feature maps ('modalities') fed into the model. Overall, across these, the right hemisphere (51.7%) and the left hemisphere (48.3%) showed equal

contributions. Single modality contributions were as follows: EEG R (35.0%) > EEG L (33.2%) > rs-fMRI R (11.2%) > rs-fMRI L (9.6%) > task-fMRI R (3.5%) > task-fMRI L (3.4%) > structure L (2.1%) > structure R (2.1%). **Abbreviations:** IC=independent component; L=left; R=right.



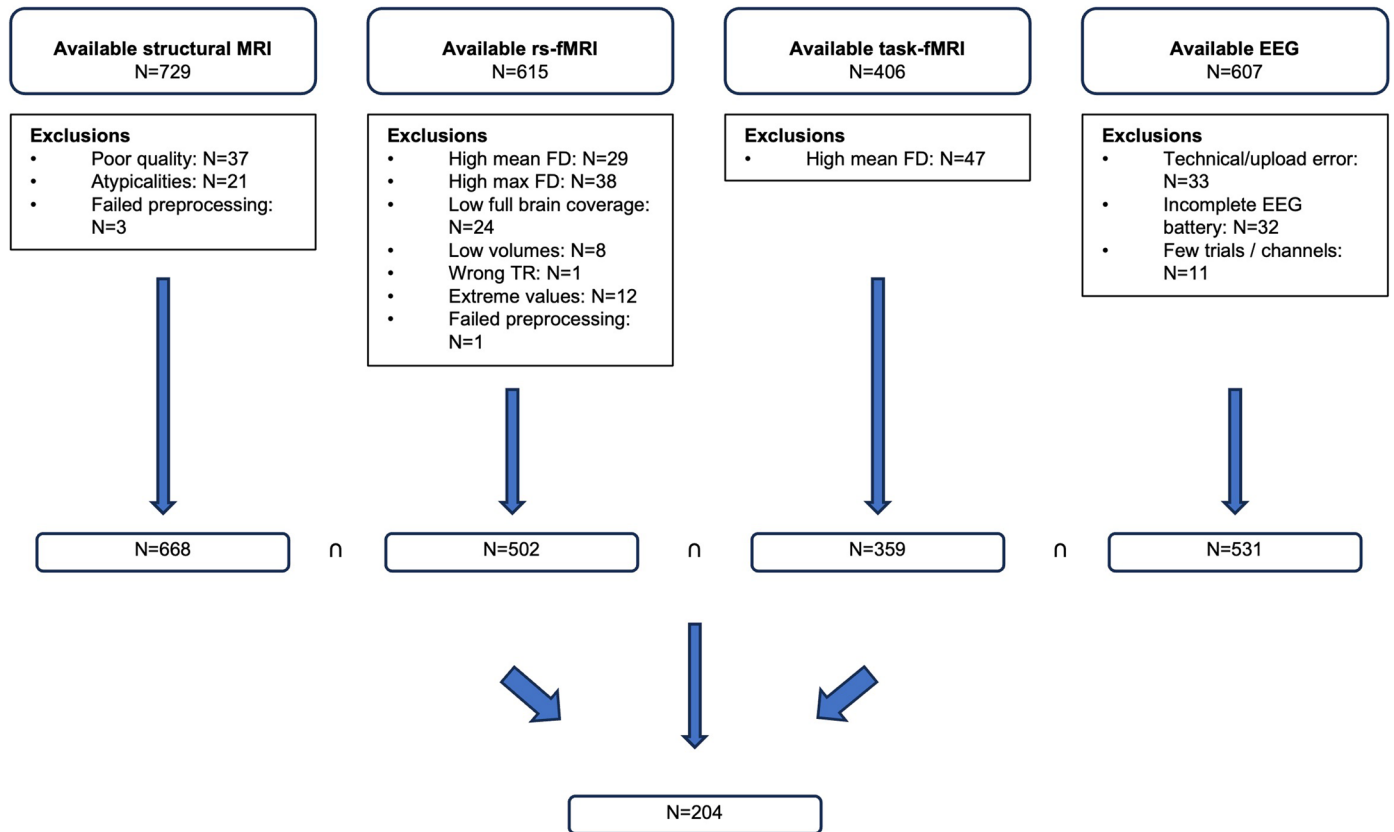
**Extended Data Fig. 3 | Support Vector Machine classification.** We ran a support vector machine (SVM) classification algorithm to test whether the multimodal independent components (ICs) outperformed the unimodal ICs in discriminating autistic from nonautistic individuals. **a)** Data are presented as the area under the receiver operating characteristic curve (AUC) along with the 95% confidence interval (CI) as a function of different thresholds between 85% to 99%

that define whether an IC is multimodal or unimodal. **b)** Data are presented as the AUC along with the 95% CI when forcing uni- and multimodal features to have the same number of ICs in each fold. In the beginning (up to six ICs) there are no differences, which become apparent when increasing the number of ICs included as features. **Abbreviations:** IC=independent component; AUC=area under the receiver operating characteristic curve; CI=confidence interval.



**Extended Data Fig. 4 | Canonical correlation analysis between the multimodal ICs and nonsocial features.** The multivariate association (that is, canonical correlation) was not significant between the eleven multimodal independent components (ICs) and the nonsocial features associated with autism ( $r = 0.45$ ,  $p\text{FDR} = 0.64$ ). Panel **a** shows the loadings of each multimodal component contributing to the CCA mode, while panel **b**) shows the loadings

of each nonsocial feature contributing to the CCA mode. Panel **c** shows the canonical correlation scatterplot color-coded by the highest contributing nonsocial feature (ADOS RRB). The x-axis depicts the projected behavioral CCA variate and the y-axis the multimodal ICs CCA variates. **Abbreviations:** IC=independent component; CCA=canonical correlation analysis.



**Extended Data Fig. 5 | Flowchart and exclusion criteria per imaging modality.** Each imaging modality had a different amount of data available. Different exclusion criteria within modality could apply to several subjects; reported numbers are thus intersecting. **Abbreviations:** FD=framewise displacement in mm.



## Reporting Summary

Nature Portfolio wishes to improve the reproducibility of the work that we publish. This form provides structure for consistency and transparency in reporting. For further information on Nature Portfolio policies, see our [Editorial Policies](#) and the [Editorial Policy Checklist](#).

### Statistics

For all statistical analyses, confirm that the following items are present in the figure legend, table legend, main text, or Methods section.

n/a Confirmed

- The exact sample size ( $n$ ) for each experimental group/condition, given as a discrete number and unit of measurement
- A statement on whether measurements were taken from distinct samples or whether the same sample was measured repeatedly
- The statistical test(s) used AND whether they are one- or two-sided  
*Only common tests should be described solely by name; describe more complex techniques in the Methods section.*
- A description of all covariates tested
- A description of any assumptions or corrections, such as tests of normality and adjustment for multiple comparisons
- A full description of the statistical parameters including central tendency (e.g. means) or other basic estimates (e.g. regression coefficient) AND variation (e.g. standard deviation) or associated estimates of uncertainty (e.g. confidence intervals)
- For null hypothesis testing, the test statistic (e.g.  $F$ ,  $t$ ,  $r$ ) with confidence intervals, effect sizes, degrees of freedom and  $P$  value noted  
*Give  $P$  values as exact values whenever suitable.*
- For Bayesian analysis, information on the choice of priors and Markov chain Monte Carlo settings
- For hierarchical and complex designs, identification of the appropriate level for tests and full reporting of outcomes
- Estimates of effect sizes (e.g. Cohen's  $d$ , Pearson's  $r$ ), indicating how they were calculated

*Our web collection on [statistics for biologists](#) contains articles on many of the points above.*

### Software and code

Policy information about [availability of computer code](#)

#### Data collection

MRI data were acquired on 3T scanners: General Electric MR750 (GE Medical Systems, Milwaukee, WI, USA) at Institute of Psychiatry, Psychology and Neuroscience, King's College London, United Kingdom (KCL); Siemens Magnetom Skyra (Siemens, Erlangen, Germany) at Radboud University Nijmegen Medical Centre, the Netherlands (RUNMC); Siemens Magnetom Verio (Siemens, Erlangen, Germany) at Autism Research Centre at the University of Cambridge, United Kingdom (UCAM); Philips 3T Achieva (Philips Healthcare Systems, Best, The Netherlands) at University Medical Centre Utrecht, the Netherlands (UMCU); GE Medical Systems Signa HDxTt at the Rome University; and Siemens Magnetom Trio (Siemens, Erlangen, Germany) at Central Institute of Mental Health, Mannheim, Germany (CIMH). Three different EEG systems were used to acquire EEG data, Brainproducts Acticaps (KCL, CIMH, RUNMC), Biosemi Active-Two (UMCU) and Micromed (UCBM).

#### Data analysis

Preprocessing of imaging data fsl/5.0.6, SPM12 (<https://www.fil.ion.ucl.ac.uk/spm/software/spm12/>) and CAT12 toolbox (<https://neuro-jena.github.io/cat/>); normative modeling with Predictive Clinical Neuroscience toolkit (PCNtoolkit) software v 0.26 (<https://pcntoolkit.readthedocs.io/en/latest>) implemented in python 3.6; linked ICA ([https://github.com/allera/Llera\\_elife\\_2019\\_1/tree/master/matlab\\_flica\\_toolbox](https://github.com/allera/Llera_elife_2019_1/tree/master/matlab_flica_toolbox)) implemented in python 3.6; canonical correlation analysis implemented in MATLAB (<https://github.com/andersonwinkler/PermCCA>); support vector machine implemented in python 3.6 using scikit-learn.

For manuscripts utilizing custom algorithms or software that are central to the research but not yet described in published literature, software must be made available to editors and reviewers. We strongly encourage code deposition in a community repository (e.g. GitHub). See the Nature Portfolio [guidelines for submitting code & software](#) for further information.

## Data

Policy information about [availability of data](#)

All manuscripts must include a [data availability statement](#). This statement should provide the following information, where applicable:

- Accession codes, unique identifiers, or web links for publicly available datasets
- A description of any restrictions on data availability
- For clinical datasets or third party data, please ensure that the statement adheres to our [policy](#)

Due to privacy/confidentiality concerns and ethical/funding restrictions, the raw clinical and neuroimaging datasets generated and/or analyzed within the current study are currently not publicly available yet. Data collected in EU-AIMS LEAP are stored and curated at the EU-AIMS database. The database is only accessible to EU-AIMS members until study end and will subsequently be opened to the wider scientific community. Scripts used to implement the experimental task are covered by a material transfer agreement, which can be obtained through the corresponding author. The VIS atlas is available under [download.brainvoyager.com/data/visfAtlas.zip](https://download.brainvoyager.com/data/visfAtlas.zip). The Harvard Oxford atlas is distributed with [fsl](http://www.fmrib.ox.ac.uk/fsl/) (<http://www.fmrib.ox.ac.uk/fsl/>), for further information see [https://ftp.nmr.mgh.harvard.edu/pub/dist/freesurfer/tutorial\\_packages/centos6/fsl\\_507/doc/wiki/Atlases.html](https://ftp.nmr.mgh.harvard.edu/pub/dist/freesurfer/tutorial_packages/centos6/fsl_507/doc/wiki/Atlases.html). Source data are provided with this paper. Corresponding author contact: D.L. Floris, [Dorothea.floris@uzh.ch](mailto:Dorothea.floris@uzh.ch).

## Human research participants

Policy information about [studies involving human research participants and Sex and Gender in Research](#).

|                             |   |
|-----------------------------|---|
| Reporting on sex and gender | Sex was considered in normative modeling and CCA as covariate.  |
| Population characteristics  | All autistic participants had an existing clinical diagnosis of autism according to DSM-IV, DSM-IV-TR, DSM-5 or ICD-10 criteria. In the autism group, diagnosis was confirmed using the combined information of gold-standard diagnostic instruments, the Autism Diagnostic Interview-Revised (ADI-R) and the Autism Diagnostic Observation Schedule (ADOS). The final sample had both complete imaging data across four different imaging modalities and phenotypic information available consisting of 99 autistic (71 males, 28 females) and 105 NAI (71 males, 34 females) between 7-30 years of age. |
| Recruitment                 | Participants were recruited from existing volunteer databases, existing research cohorts, clinical referrals from local outpatient centres, special needs schools, mainstream schools and local communities.  |
| Ethics oversight            | The study was approved by the local ethical committees of participating centres (see Supplementary Table 9), and written informed consent was obtained from all participants or their legal guardians (for participants <18 years).   |

Note that full information on the approval of the study protocol must also be provided in the manuscript.

## Field-specific reporting

Please select the one below that is the best fit for your research. If you are not sure, read the appropriate sections before making your selection.

Life sciences       Behavioural & social sciences       Ecological, evolutionary & environmental sciences

For a reference copy of the document with all sections, see [nature.com/documents/nr-reporting-summary-flat.pdf](https://nature.com/documents/nr-reporting-summary-flat.pdf)

## Life sciences study design

All studies must disclose on these points even when the disclosure is negative.

|                 |  |
|-----------------|--|
| Sample size     | No sample size calculation was performed. All available data from EU-AIMS LEAP was used to maximize sample size. The final sample of 204 individuals (99 autistic individuals, 105 non-autistic individuals) was selected to have both complete imaging data across four different imaging modalities and phenotypic information available.  |
| Data exclusions | <ul style="list-style-type: none"> <li>• Structural T1-weighted images with excessive head motion (N=37), clinically (mostly) non-significant atypicalities (N=21) and failed preprocessing (N=3) were excluded.</li> <li>• Resting-state fMRI data (rs-fMRI) was available for five out of the six acquisition sites (not collected for the Rome site). Scans with fewer than 180 volumes (i.e., fewer than 90% of R-fMRI scan completed; N=8), a TR different than the standard TR =2.3 (N=1), excessive head motion during the R-fMRI scan (N=29 with mean root-mean-square of the framewise displacement [meanFD] &gt;0.7mm and N=38 with maxFD &gt;7.6mm [i.e., motion of more than 2 voxels]), low full-brain coverage (N=24), extreme values (N=12 with values &gt;4SD) and failed preprocessing (N=1) were excluded.</li> <li>• Hariri task-fMRI datasets with excessive head motion (&gt;20% of trials with a meanFD greater than 0.5mm; N=47) were excluded.</li> <li>• EEG data was available for five out of the six acquisition sites (not collected for the Cambridge site). Images with technical/upload errors (N=33), incomplete EEG battery (N=32), too few trials (&lt;20 artifact-free; N=9) and too few channels (&lt;75%; N=2) were excluded.</li> </ul> |
| Replication     | Normative modeling was replicated modeling age linearly. Several sensitivity analyses corroborated primary analyses. These included: a) To evaluate the robustness of our selected model order (N=50), we re-ran LICA using different dimensional factorizations of subject loadings (N=40 and N=60) and computed correlations among them. Different model orders were similar to each other; b) To test for robustness of the   |

SVM results, we showed that results were stable across different thresholds resulting in slightly varying degrees of multimodality ranging between 85% to 99% of single modality contributions. Given that each threshold resulted in a different number of unimodal vs. multimodal components, we further showed that results remained stable when forcing uni- and multimodal components to have the same number of features ; c) To assess robustness of CCA results, we set a range of multimodal thresholds between 85% to 99% and selected ICs with modality contributions exceeding this threshold. We showed that associations remained stable when re-running the CCA using varying degrees of multimodality.

**Randomization** While diagnosis cannot be randomized and there was no allocation to experimental groups, in normative modeling, and SVM analyses, randomization was used to divide data into independent training and validation sets.

**Blinding** Blinding for imaging acquisition was not applicable/relevant. Randomized allocation of data to training and validation sets in normative modeling and SVM. Furthermore, linked ICA was blind to diagnostic labels.

## Reporting for specific materials, systems and methods

We require information from authors about some types of materials, experimental systems and methods used in many studies. Here, indicate whether each material, system or method listed is relevant to your study. If you are not sure if a list item applies to your research, read the appropriate section before selecting a response.

### Materials & experimental systems

|                                     |                          |                               |
|-------------------------------------|--------------------------|-------------------------------|
| n/a                                 | <input type="checkbox"/> | Involvement in the study      |
| <input checked="" type="checkbox"/> | <input type="checkbox"/> | Antibodies                    |
| <input checked="" type="checkbox"/> | <input type="checkbox"/> | Eukaryotic cell lines         |
| <input checked="" type="checkbox"/> | <input type="checkbox"/> | Palaeontology and archaeology |
| <input checked="" type="checkbox"/> | <input type="checkbox"/> | Animals and other organisms   |
| <input checked="" type="checkbox"/> | <input type="checkbox"/> | Clinical data                 |
| <input checked="" type="checkbox"/> | <input type="checkbox"/> | Dual use research of concern  |

### Methods

|                                     |                                     |                          |
|-------------------------------------|-------------------------------------|--------------------------|
| n/a                                 | <input type="checkbox"/>            | Involvement in the study |
| <input checked="" type="checkbox"/> | <input type="checkbox"/>            | ChIP-seq                 |
| <input checked="" type="checkbox"/> | <input type="checkbox"/>            | Flow cytometry           |
| <input type="checkbox"/>            | <input checked="" type="checkbox"/> | MRI-based neuroimaging   |

## Magnetic resonance imaging

### Experimental design

|                                 |   |
|---------------------------------|---|
| Design type                     | <ul style="list-style-type: none"> <li>• Structural MRI: T1-weighted images were obtained using a 5.5 minute MPRAGE sequence; • Resting-state fMRI: An eight-to- ten minute rs-fMRI scan was acquired using a multi-echo planar imaging (ME-EPI) sequence; • Task-fMRI: Data were acquired with echo-planar T2*-weighted imaging (EPI), sensitive to the Blood Oxygenation Level Dependent (BOLD) signal contrast; • EEG: Three different EEG systems were used to acquire the data, Brainproducts Acticaps (KCL, CIMH, RUNMC), Biosemi Active-Two (UMCU) and Micromed (UCBM).</li> </ul> |
| Design specifications           | n.a.  |
| Behavioral performance measures | Hariri face matching task   |

### Acquisition

|                               |  |
|-------------------------------|--|
| Imaging type(s)               | Structural, functional (task- and resting-state), EEG  |
| Field strength                | 3T   |
| Sequence & imaging parameters | <ul style="list-style-type: none"> <li>• T1-weighted images: images were obtained using a 5.5 minute MPRAGE sequence (Nijmegen site example: TR=2300ms, TE=2.93ms, T1=900ms, voxels size=1.1x1.1x1.2mm, flip angle=9°, matrix size=256x256, FOV=270mm, 176slices).</li> <li>• Resting-state fMRI: An eight-to- ten minute rs-fMRI scan was acquired using a multi-echo planar imaging (ME-EPI) sequence, TR=2300ms, TE~12ms, 31ms, and 48ms (slight variations are present across centres), flip angle=80°, matrix size=64x64, in-plane resolution=3.8mm, FOV=240mm, 33 axial slices, slice thickness/gap=3.8mm/0.4mm, volumes=200 (UMCU), 215 (KCL, CIMH), or 266 (RUNMC, UCAM).</li> <li>• Task-fMRI: Data were acquired with echo-planar T2*-weighted imaging (EPI), sensitive to the Blood Oxygenation Level Dependent (BOLD) signal contrast. We used a well-established task that probe functional brain responses during socio-emotional information processing.</li> <li>• EEG: five sites acquired EEG data in LEAP. Three different EEG systems were used to acquire the data, Brainproducts Acticaps (KCL, CIMH, RUNMC), Biosemi Active-Two (UMCU) and Micromed (UCBM). Across all sites, 70 EEG channels with standard positions were used.</li> </ul> |
| Area of acquisition           | Whole brain  |
| Diffusion MRI                 | <input type="checkbox"/> Used <input checked="" type="checkbox"/> Not used   |

## Preprocessing

|                            |  |
|----------------------------|--|
| Preprocessing software     | fsl/5.0.6; SPM12, CAT12 toolbox  |
| Normalization              | <ul style="list-style-type: none"> <li>• T1-weighted images: we created a study-specific template with DARTEL (i.e., a nonlinear diffeomorphic registration algorithm) and segmented images were registered to MNI space.</li> <li>• Resting-state fMRI: The T1 images of each participant were registered to MNI152 standard space using 12-parameter affine transformation and refined using non-linear registration with FSL FNIRT (10mm warp, 2mm resampling resolution). Finally, we brought all participant-level rs-fMRI images to 2mm MNI152 standard space by applying the rs-fMRI to T1 and T1 to MNI152 transformations.</li> <li>• Task-fMRI: normalization to standard stereotactic space as defined by the Montreal Neurological Institute.</li> </ul> |
| Normalization template     | MNI152 standard space template   |
| Noise and artifact removal | <ul style="list-style-type: none"> <li>• Resting-state fMRI: we thoroughly corrected for secondary head-motion related artifacts, by applying ICA-AROMA, an ICA-based method, which automatically detects and removes motion-related components from the data. ICA-AROMA has been demonstrated to remove head motion-related artifacts with high accuracy while preserving signal of interest. We applied nuisance regression to remove signal from white matter and cerebrospinal fluid.</li> <li>• EEG: Data were cleaned in Matlab with single trials with whole scalp artefacts and EOG artefacts being excluded.</li> </ul>   |
| Volume censoring           | n.a.   |

## Statistical modeling & inference

|   |   |
|---|---|
| Model type and settings   | Bayesian Linear Regression under 10-fold cross-validation; multivariate (Bayesian) linked independent component analysis; multivariate canonical correlation; general linear models   |
| Effect(s) tested  | Linked grey matter volume deviations, task-activation deviations, resting-state functional connectivity deviations, source activation deviations. Classification performance difference between unimodal and multimodal component. Multivariate association with social-communicative features. |
| Specify type of analysis:   | <input type="checkbox"/> Whole brain <input checked="" type="checkbox"/> ROI-based <input type="checkbox"/> Both  |
| Anatomical location(s)  | Fusiform Gyrus based on Harvard Oxford atlas.   |
| Statistic type for inference<br>(See <a href="#">Eklund et al. 2016</a> ) | Voxel-wise  |
| Correction  | False Discovery Rate  |

## Models & analysis

|   |   |
|---|---|
| n/a   | Included in the study   |
| <input type="checkbox"/>                      | <input checked="" type="checkbox"/> Functional and/or effective connectivity  |
| <input checked="" type="checkbox"/>           | <input type="checkbox"/> Graph analysis   |
| <input type="checkbox"/>                      | <input checked="" type="checkbox"/> Multivariate modeling or predictive analysis  |
| Functional and/or effective connectivity      | seed-based connectivity analysis (rs-fMRI)  |
| Multivariate modeling and predictive analysis | <p>Normative models were trained across all individuals using Bayesian Linear Regression (BLR) using PCNtoolkit package (version 0.26) (<a href="https://pcntoolkit.readthedocs.io/en/">https://pcntoolkit.readthedocs.io/en/</a>) modelling the relationship between each brain imaging modality (within the right and left FFG ROI) and age, sex and scanning site. Normative models were derived in an unbiased manner under 10-fold cross-validation. This Bayesian approach calculates the probability distribution over all functions that fit the data while specifying a prior over all possible values and relocating probabilities based on evidence (i.e., observed data). As such, it yields unbiased estimates of generalizability and inferences with increasing uncertainty with fewer data. In primary analysis, a B-spline basis expansion of the of covariate vector was used to model non-linear effects of age. We compared model performance with that of modelling age linearly (without a B-spline basis expansion). To merge modalities, Linked Independent Component Analysis (LICA) was used. This is a Bayesian extension of single modality ICA model which provides an automatic decomposition of the brain features into independent components (ICs) that characterize the inter-subject brain variability. These multiple decompositions share a mixing matrix or subject course across individual feature factorizations that reflect the subject contributions to each independent component. To assess whether multimodal components outperformed unimodal components in discriminating autistic from non-autistic individuals, we implemented a Support Vector Machine (SVM) classification algorithm under 10-fold cross-validation using scikit-learn in Python. To model the multivariate relationship between the identified multimodal ICs and cognitive features related to social functioning and face processing in autism, we ran canonical correlation analysis (CCA)</p> |